Extension of the Representative Elementary Watershed approach for cold regions: constitutive relationships and an application

L. Mou, F. Tian, H. Hu, M. Sivapalan

Hydrol. Earth Syst. Sci. Discuss., 4, 3627–3686, 2007
www.hydrol-earth-syst-sci-discuss.net/4/3627/2007/

Hydrology and Earth System Sciences Discussions

Papers published in *Hydrology and Earth System Sciences Discussions* are under open-access review for the journal *Hydrology and Earth System Sciences*

Extension of the Representative Elementary Watershed approach for cold regions: constitutive relationships and an application

L. Mou[1], F. Tian[1], H. Hu[1], and M. Sivapalan[2]

[1]State Key Laboratory of Hydroscience and Engineering, Department of Hydraulic Engineering, Tsinghua University, China
[2]Departments of Geography & Civil and Environmental Engineering, University of Illinois at Urbana-Champaign, USA

Received: 21 September 2007 – Accepted: 25 September 2007 – Published: 2 October 2007

Correspondence to: F. Tian (tianfq@tsinghua.edu.cn)

Abstract

The representative elementary watershed (REW) approach proposed by Reggiani et al. (1998, 1999) represents an attempt to develop a scale adaptable modeling framework for the hydrological research community. Tian et al. (2006a) extended the original REW theory for cold regions through explicit treatment of energy balance equations to incorporate associated cold regions processes, such as melting and accumulation of glacier and snow, and freezing and thawing of soil ice. However, constitutive relationships for the cold regions processes needed to complete these new balance equations have been left unspecified in this derivation. In this paper we propose a set of closure scheme for cold regions processes within the extended framework provided by Tian et al. (2006a). A rigorous energy balance method is proposed to close the balance equations of melting/accumulation processes as well as the widely-used and conceptual degree-day method, whereas the closure schemes for soil freezing and thawing are based on the "maximum unfrozen-water content" model. The proposed closure schemes are coupled to the previously derived balance equations and implemented within Thermodynamic Watershed Hydrological Model (THModel, Tian, 2006b) and then applied to the headwaters of the Urumqi River in Western China. The results of the 4-year calibration and 1-year validation analyses show that THModel can indeed simulate runoff processes in this snow and glacier-dominated catchment very well, which confirms the applicability of the modeling based on the REW approach and the validity of the developed closure schemes for cold regions processes.

1 Introduction

Prediction of hydrological responses at the catchment scale in a changing environment, such as due to natural and human induced climate and landscape changes, is a grand challenge in the hydrological sciences, and is of crucial importance for sustainable water management and hazard mitigation. The current generation of physically based,

HESSD

4, 3627–3686, 2007

distributed hydrological models for the upscaling of point-scale balance equations, as set out by Freeze and Harlan (1969), have the drawback that there is no a priori perception about how the micro-scale processes interact with each other (Sivapalan, 2003a) and therefore cannot account for the self-organized features that emerge at the macro-scale, i.e., catchment scale, as a result of these interactions (McDonnell et al., 2007). One of the most obvious emergent features frequently recognized in the literature is preferential flow which results from the interactions of subsurface flow, soil and biota, and cannot be easily handled using traditional micro-scale process descriptions. Models such as SHE (Abbott et al., 1986), THIHMS-SW (Ni et al., 2007), among many others, are often criticized for their excessive complexity and parameter identifiability in comparison with limited data availability and excessive computational demands.

The Representative Elementary Watershed (REW) approach first proposed by Reggiani et al. (1998, 1999) provides a general framework to incorporate all possible emergent behaviors of the hydrological system parameterized directly at the catchment scale. It invokes mass, momentum, and energy conservation equations and entropy constraints directly at the scale of the so called representative elementary watersheds (REWs), which are by themselves macro-scale discrete units. By coupling appropriate closure relationships to these balance equations to make the system of governing equations determinate, the REW approach has the potential to represent the net effects of the spatial and temporal heterogeneity of micro-scale processes (Lee et al., 2007), including the effects of self-organizing features that emerge at the macro-scale without any conceptual jump or inconsistency. For these reasons we argue, as do Reggiani and Schellekens (2003) and Reggiani and Rientjes (2005), that the REW approach can serve as an alternative blueprint compared to the classical Freeze and Harlan (1969) blueprint, providing a key building block to a general modeling framework when combined with the alternative downward approach to modeling (Sivapalan et al., 2003b).

As mentioned before, the set of balance equations arising from the REW approach, on their own, are indeterminate, i.e., they have more unknowns than equations. In

other words, the states of the system and the flux exchanges cannot be determined just through the use of the conservative principles quite common in continuum mechanics. They have to be supplemented by additional equations, including geometric and constitutive relationships, to make the final set of balance equations determinate (Tian et al., 2006a). This issue is usually called the closure problem (Zhang et al., 2005b) which lies at the heart of the REW approach, as pointed out by Beven (2002, 2006). In the original work of Reggiani et al. (1998, 1999), each REW is divided into five sub-regions (zones), i.e., an unsaturated zone (u-zone), a saturated zone (s-zone), a concentrated overland flow zone (c-zone), a saturated overland flow zone (o-zone), and the main channel reach (r-zone). Remaining within this system definition, several researchers have proposed different closure schemes and have applied them to hypothetical and real watersheds. Reggiani and Rientjes (2005) developed a model in which constitutive relationships were deduced by using the Coleman-Noll procedure (Coleman and Noll, 1963) and the Hardy Cross method (Cross, 1936). Reggiani et al. (2000, 2001) subsequently demonstrated the applicability of the REW approach and the corresponding closure schemes in hypothetical and real watersheds (Reggiani and Rientjes, 2005). Zhang et al. (2005b) introduced an interception component and developed a multi-layer soil column definition for the REW formulation, and applied the resulting REWASH model to Geer (2005a), Alzette (2006), Zwalm (Taibi et al., 2006) watersheds in Europe. Lee et al. (2007) and Tian (2007) surveyed the variety of methods in use for developing the constitutive relationships, and classified them into two primary types, namely, the experimental method and the statistical method. Of these, the former is based on direct regression analysis of laboratory and/or field experimental results, and the latter is based on the upscaling of micro-scale process understanding to the macro-scale, similar to statistical mechanics. With the help of the fully physically based, distributed hydrological model, CATFLOW (Zehe et al., 2001), Lee et al. (2007) proposed a closure scheme that was different from Reggiani and Rientjes (2005) and Taibi et al. (2006), by explicitly considering spatial heterogeneity of soil properties. Tian (2006b) obtained similar results by coupling the Monte Carlo simulation approach and

the 1-D Richards' equation. On the basis of the closure relations developed through up-scaling of the CATFLOW model, Lee et al. (2005) developed the CREW model and applied it to the Weiherbach watershed in Germany and Susannah Brook watershed in Australia.

Despite all this progress, the original REW approach as set out by Reggiani *et al.* (1998, 1999) cannot fully account for energy related processes, especially in cold regions which exhibit a complex hydrological regime. In fact, cold regions cover nearly half of the global land area (Yang et al., 2000), at least during the cold season, and the water that melts from glaciers and the snowpack account for a significant component of daily water supply in cold regions (McManamon et al., 1993; Williams and Tarboton, 1999). Hydrological processes in cold regions are strongly influenced by energy storage and transfer processes, which, so far, cannot be represented within Reggiani et al. (1998, 1999) original formulation of the REW approach. By re-defining the structure and composition of the REW, Tian et al. (2006a) have extended the Representative Elementary Watershed approach for cold regions. In their revised formulation, each REW is partitioned into six surface sub-regions and two subsurface sub-regions. Vegetation, snow, soil ice, and glacier ice are added to the existing system that included water, gas, and soil matrix. As a result, energy related processes i.e., evaporation/transpiration, accumulation and depletion of snowpack and glacier, and the freezing and thawing of soil ice, can be modeled in a physically reasonable way. The Thermodynamic Hydrological Model (THModel) has been developed by adopting Lee et al.'s (2007) closure scheme within this new extended REW formulation and applied to the semi-arid experimental watershed (Chabagou River basin) in China with good results (Tian, 2006b; Tian et al., 2007). However, up till now the closure schemes incorporated in the model completely exclude the energy balance equations and constitutive relationships appropriate for cold regions processes have not been developed within the REW framework. This paper will serve as a companion paper to Tian et al. (2006a) and aims to develop parsimonious parameterizations for the melting and accumulation of glacier and snow, freezing and thawing of soil ice by taking full advantage of energy balance equations,

and to demonstrate the capability of a generalized cold regions REW-based model for long-term streamflow modeling in high mountainous cold regions.

The remainder of this paper is organized as follows. In Sect. 2 we give a brief review of the balance equations, along with a few necessary but minor revisions and existing closure relationships for non-cold regions, as present in the existing THModel. Following this, in Sect. 3, we will propose appropriate constitutive relationships for the glacier zone, snow covered zone, and soil ice within the unsaturated zone, which will make the coupled balance equations fully determinate. This will be followed up, in Sect. 4, by a case study involving the application of the new THModel to a headwater catchment of the Urumqi River Basin located in northwest of China, and a discussion of the results of model application. This will be followed, in Sect. 5, by a summary of the main results and conclusions.

2 Brief review of THModel

In the THModel (Tian et al., 2006a, 2007), the REW is divided into surface layer and subsurface layer (see Fig. 1). Six sub-regions (or zones) are defined in the surface layer, i.e., a bare soil zone (b-zone), vegetated zone (v-zone), a snow covered zone (n-zone), a glacier covered zone (g-zone), a sub-stream-network (t-zone), and the main channel reach (r-zone), while two sub-regions are defined in the sub-surface layer, i.e., an unsaturated zone (u-zone) and a saturated zone (s-zone). The ice phase is introduced into both the u-zone and s-zone to allow soil freezing and thawing to be modeled.

The mass, momentum, energy balance equations for each zone are derived in a systematic and extensible way by Tian et al. (2006a). In the interest of consistence, we will here list the special balance equations for cold regions including the equations for g-zone, n-zone, and u-zone, and make some minor revisions on them for later use. In frozen areas the saturated zone is considered to be beneath the frozen soil layer and mass exchange rate between s-zone and other sub-regions is rather slow (Lin, 1980).

As a first attempt, the balance equations for s-zone are, therefore, ignored in this paper. Also, we will here list the closure relationships for the constitutive variables related with non-cold processes. For details about the balance equations for other sub-regions and the established closure relationships please refer to Tian et al. (2006a, 2007), and about the symbols in the following equations please refer to the nomenclature.

2.1 Balance equations for the glacier zone

(1) Mass balance equation for water

$$e_l^{gT} + e_l^{gu} + e_l^{gt} + e_{lg}^{g} + e_{li}^{g} = 0 \tag{1}$$

where the terms on the l.h.s. account for the intensity of rainfall, infiltration or exfiltration, runoff, evaporation, and melting or freezing, respectively.
(2) Mass balance equation for ice

$$\frac{d}{dt}(\overline{\rho_i^g} y^g \omega^g) = e_i^{gT} + e_{ig}^{g} + e_{il}^{g} \tag{2}$$

where the l.h.s term accounts for the rate of change of the glacier ice storage, and the terms on the r.h.s. represent the intensity of snowfall, and the rates of sublimation and freezing, respectively.

Snowfall and rainfall often occur simultaneously and therefore cannot be easily separated. Also, we cannot easily calculate evaporation and sublimation separately. We therefore combine Eqs. (1) and (2) together, which yields

$$\frac{d}{dt}(\overline{\rho_i^g} y^g \omega^g) = e_l^{gT} + e_i^{gT} + e_l^{gu} + e_l^{gt} + e_{lg}^{g} + e_{ig}^{g} \tag{3}$$

The water exchange between g-zone and u-zone (e_l^{gu}) is usually small and can be omitted, and for the reason of simplicity, we use a new symbol, e^{gT}, to donate total

precipitation, $e_l^{gT}+e_i^{gT}$, and combine two phase transition terms, i.e., ice melting (e_{lg}^g) and sublimation (e_{ig}^g), into a single term $e_{(l,i)g}^g$, which is usually called glacier surface evaporation and denoted by e_{lg}^g. Therefore, the mass balance equation for the whole glacier zone can be re-written as follows:

$$\frac{d}{dt}(\overline{\rho_i^g} y^g \omega^g) = e^{gT} + e_l^{gt} + e_{lg}^g \tag{4}$$

(3) Heat balance equation for the glacier zone

$$y^g \omega^g c^g \frac{d}{dt}\overline{T^g} = l_{lg} e_{lg}^g + l_{ig} e_{ig}^g + l_{il} e_{il}^g + \overline{R_n^g}\omega^g + Q^{gT} + Q^{gu} + Q^{gt}\text{“} \ [1] \tag{5}$$

where the l.h.s. term represents the rate of change of heat storage, the terms on the r.h.s. are the rate of latent heat of vaporization, sublimation, and fusion, net radiation intensity, and rates of heat exchange with the atmosphere, u-zone, and t-zone, respectively.

Following the assumption made previously that e_l^{gu} in Eq. (3) is usually small and can be neglected, the term Q^{gu} can be similarly omitted. Similarly, the two latent heat terms, i.e., $l_{lg}e_{lg}^g$ and $l_{ig}e_{ig}^g$, are combined into a single term donated by $l'_{lg}e_{lg}^g$, where e_{lg}^g is the glacier surface evaporation and l'_{lg} will be defined later in Sect. 3.1. With these assumptions, the heat balance equation (Eq. 5) can be simplified as follows:

$$y^g \omega^g c^g \frac{d}{dt}\overline{T^g} = l'_{lg} e_{lg}^g + l_{il} e_{il}^g + \overline{R_n^g}\omega^g + Q^{gT} + Q^{gt} \tag{6}$$

[1] In this paper we use T to denote the temperature other than θ in Tian et al. (2006a) (not to be confused with the vector symbol $\boldsymbol{T}$ to denote the momentum term).

2.2 Balance equations for the snow zone

(1) Mass balance equation for water phase

$$\frac{d}{dt}(\overline{\rho_l^n}\varepsilon_l^n y^n \omega^n) = e_l^{nT} + e_l^{nu} + e_l^{nt} + e_{lg}^n + e_{ln}^n \quad (7)$$

where the l.h.s. represents the rate of change of water storage, the terms on the r.h.s. represent the intensity of rainfall, rate of water exchange with the u-zone, with the t-zone, with the vapor phase (i.e., evaporation), and with the snow phase (i.e. melting), respectively.

(2) Mass balance equation for snow phase

$$\frac{d}{dt}(\overline{\rho_n^n}\varepsilon_n^n y^n \omega^n) = e_n^{nT} + e_{ng}^n + e_{nl}^n \quad (8)$$

where the l.h.s. term is the rate of change of snow storage, the terms on the r.h.s. represent the intensity of snowfall, rate of snow exchange with the vapor phase (i.e., sublimation) and with the water phase (i.e. melting).

Very similar to the g-zone, we can obtain the combined mass balance equation for the snow zone as follows:

$$\frac{d}{dt}(\overline{\rho^n} y^n \omega^n) = e^{nT} + e_l^{nu} + e_l^{nt} + e_{lg}^n \quad (9)$$

where the l.h.s. term represents the change rate of total mass including snow and water in the n-zone, $\overline{\rho^n}$ is the average density of snow and water in snow-pack, y^n is the equivalent depth of the n-zone, and ω^n is the area fraction of the n-zone, e^{nT} is total precipitation, i.e., $e_l^{nT} + e_n^{nT}$, and the the last term on the r.h.s. is the combination of e_{lg}^n and e_{ln}^n in Eq. (6), which is denoted by e_{lg}^n. The meaning of other symbols is similar to those of Eqs. (6) and (7).

(3) Heat balance equation for the snow zone

$$y^n \omega^n c^n \frac{d}{dt}\overline{T^n} = I_{lg} e_{lg}^n + I_{ng} e_{ng}^n + I_{nl} e_{nl}^n + \overline{R_n^n}\omega^n + Q^{nT} + Q^{nu} + Q^{nt} \quad (10)$$

where, the term on the l.h.s. is the rate of change of heat storage, the first three terms on the r.h.s. represent the rate of latent heat transfer of vaporization, of sublimation, and of fusion, respectively, and the remaining terms on the r.h.s. represent the net radiant intensity, heat exchange rate with the atmosphere, with the u-zone, and with t-zone, respectively.

2.3 Balance equations for unsaturated zone

(1) Mass balance equation for water

$$\frac{d}{dt}\left(\overline{\rho_l^u}\varepsilon_l^u y^u \omega^u\right) = e_l^{uEXT} + \sum_{L=1}^{N_K} e_l^{uL} + e_l^{us} + e_l^{ub} + e_l^{uv} + e_l^{un} + e_l^{ug} + e_{li}^u \tag{11}$$

where the l.h.s. term is the rate of change of water storage, and the terms on the r.h.s. are various water exchange terms with the external world, neighboring REWs, s-zone, b-zone, v-zone, n-zone, g-zone, and ice phase, respectively.

(2) Mass balance equation for ice

$$\frac{d}{dt}\left(\overline{\rho_i^u}\varepsilon_i^u y^u \omega^u\right) = e_{il}^u = -e_{li}^u \tag{12}$$

(3) Heat balance equation for u-zone

$$\omega^u y^u c^u \frac{d}{dt}\overline{T^u} = Q^{ub} + Q^{uv} + Q^{un} + Q^{ug} + Q^{us} + l_{il} e_{il}^u \tag{13}$$

where the l.h.s. term represents the change rate of heat storage, the terms on the r.h.s. account for REW-scale heat exchange rate with b-zone, v-zone, n-zone, g-zone, and s-zone, and the rate of freezing heat, respectively.

As shown in Eq. (11), the exchange terms between u-zone and its environment and among different phases are highly complex. To confine the problem to a manageable level, we assume that (a) the depth and area ratio of u-zone are constant in the frozen

areas, (b) water exchange terms with neighboring REWs or the external world are negligible, (c) water exchange term with the g-zone is negligible as suggested in Sect. 2.1, and (d) water exchange terms with s-zone are negligible when ice coexisting with water limits water movement in the u-zone, as suggested at the beginning of this section. Also, we provide here an alternative simpler way to account for the saturation excess runoff by introducing the mass exchange term from the u-zone to the t-zone $\left(e_l^{ut}\right)$ instead of changing the area of the t-zone as done in Tian et al. (2007), which will be discussed more in Sect. 3.3. Given the above assumptions, we obtain the following equations after adding Eqs. (11) and (12) together:

$$\rho_l y^u \omega^u \frac{d}{dt}\left(\varepsilon_l^u\right) = e_l^{ub} + e_l^{uv} + e_l^{un} + e_l^{ut} - \rho_i y^u \omega^u \frac{d}{dt}\left(\varepsilon_i^u\right) \tag{14}$$

where ρ_l and ρ_i are the mass density of water and ice, respectively.

Similarly, the heat balance equation can also be rewritten as

$$\omega^u y^u c^u \frac{d}{dt}\overline{T^u} = Q^{ub} + Q^{uv} + Q^{un} + Q^{ut} + l_{il}\rho_i y^u \omega^u \frac{d}{dt}\left(\varepsilon_i^u\right) \tag{15}$$

2.4 Constitutive relationships for non-cold region hydrological processeone

Tian et al. (2007) closed the resulting set of ordinary differential equations (ODEs) by adopting Lee et al.'s (2007) closure scheme for non-cold region hydrological processes within the framework of extended REW approach. The principal closure formulae are listed in Table 1. The special constitutive relationships for the energy related processes will be developed in Sect. 3 below.

2.5 Numerical implementation of THModel

The final result of ODEs in THModel is more easily numerically solved than partial differential equations (PDEs) on which the current generation of physical hydrological

models are based. The numerical part of THModel is implemented with the help of a famous ODE solver, CVODE (Cohen and Hindmarsh, 1996), within which the iterative formula of ODEs is based on the Backward Differentiation Formulas (BDE) coupled with Newtonian Iteration for nonlinear equations and the preconditioned GMRES algorithm for linear equations.

3 Constitutive relationships for the energy related processes in cold regions

Special processes in cold regions can be classified into two types. One is the melting and accumulation of glacier and snow, which may contribute to annual or seasonal runoff and hence greatly influence the overall water balance, and the others are the freezing and thawing of soil water which may alter soil properties and hence dramatically influence water and energy transfers in unsaturated zone. Both of them are driven by relevant energy processes, which are primarily heat processes. These contribute to the intimate and complex coupling between water and heat transfer and storage processes.

Generally speaking, both snow and glacier melting processes are subject to similar driving forces, i.e., the solar radiation and sensible heat flux. We can close the balance equations of the g-zone and n-zone by explicitly considering the energy transfer processes in a rigorous manner, which is called energy balance method in this paper (see Sect. 3.1 below). It is, however, always difficult in practice to apply the energy balance method to model snow melt for long-term, large-scale applications owing to the large heterogeneity of snow distribution in space and time, the complex structure of snowpack and limited data in cold, remote regions. A simpler method using the widely-used degree-day formula is, therefore, then introduced to provide an alternative approach to close the n-zone balance equations (see Sect. 3.2 below).

Mass and energy exchange terms among different sub-regions are illustrated in Fig. 2 and the detailed one for the n-zone is shown in Fig. 3.

3.1 Energy balance method for closing glacier/snow melting and accumulation equation

Mass and energy terms are intimately coupled during glacier/snow melting and accumulation processes, which can be clearly seen from the mass balance equations, Eqs. (4) and (9) for g-zone and n-zone respectively, and the corresponding heat balance equations, Eqs. (6) and (10), respectively. In order to close the balance equations, we must specify all the redundant unknowns in a physically reasonably way. In the interest of simplicity, we will take the g-zone as an example in the following section while the same method can be applied to the n-zone without too many changes.

For the balance equations in the g-zone, i.e., Eqs. (4) and (6), we take the variables $\left(y^g, \overline{T^g}\right)$ as independent unknowns, and assume that the g-zone area variation (ω^g) is rather small and hence can be ignored over hydrological time scales. The dependent unknowns are therefore $\left(e^{gT}, e_l^{gt}, e_{lg}^g, e_{il}^g, \overline{R_n}, Q^{gT}, Q^{gt}\right)$, which can be specified in terms of driving forces (i.e., observations) or through appropriate closure relationships.

(1) Precipitation (e^{gT})

e^{gT} may be either rainfall or snowfall depending on a certain critical temperature which can be given by experimental data or by calibration.

(2) Areal average net radiation intensity ($\overline{R_n^g}$)

The net radiation varies with extraterrestrial radiation, sunshine duration and terrain features in the watershed. The areal average net radiation can be estimated by GIS software (Lalit et al., 1997). For simplicity, we calculate using Eq. (16) as follows:

$$\overline{R_n^g} = R_n^g c_{rn}^g \tag{16}$$

where R_n^g is the local net radiation intensity absorbed at a representative position with mean elevation, slope and aspect in the g-zone. c_{rn}^g is a coefficient which incorporates the influence of terrain factors including slope, aspect, and hill-shade on solar radiation as well as the spatial heterogeneity within the REW. R_n^g is affected by both surface solar radiation and long-wave radiation released from the ground, which can be calculated as follows.

$$R_n^g = c_n \left(R_s^g \times (1 - \alpha^g) - R_{nl}^g \right) \tag{17}$$

where R_s^g is the local surface solar radiation ($MJm^{-2}day^{-1}$), and R_{nl}^g is local net long-wave radiation ($MJm^{-2}day^{-1}$), α^g is the albedo of the glacier, c_n is the coefficient of unit transformation from ($MJm^{-2}day^{-1}$) to (kWm^{-2}).

The surface solar radiation is determined by the extraterrestrial radiation, sunshine duration, and also the geographic location. The formula recommended by Shuttleworth (1993) and Allen et al. (1998) is adopted in this paper as follows:

$$R_s^g = \left(a_s + b_s \frac{n_{\text{sun}}}{N_{\text{sun}}} \right) R_a \tag{18}$$

$$R_a = 37.586 d_r \left(\omega_s \sin\varphi \sin\delta + \cos\varphi \cos\delta \sin\omega_s \right) \tag{19}$$

where R_a is the daily extraterrestrial radiation ($MJm^{-2}day^{-1}$), n_{sun} is the actual duration of sunshine (hour), N_{sun} is the maximum possible duration of sunshine or daylight hours (hour), a_s is a regression constant indicating the fraction of extraterrestrial radiation reaching the earth on overcast days, i.e., n_{sun}=0, a_s+b_s is the fraction of extraterrestrial radiation reaching the earth on a clear day, i.e., n_{sun}=N_{sun}, d_r is the inverse relative distance Earth-Sun, ω_s is the sunset hour angle, φ is the latitude, δ is the solar declination,

The albedo α^g depends on the characteristics of glacier surface including wetness, grain size, snow age, snow depth, and snow density (Anderson, 1976), although a good relationship between α and daily air temperature can be found. For example, Kang et al. (1992) proposed the following empirical formulae to estimate daily averaged albedo on the basis of observed air temperature in the headwaters of the Urumqi River, which will be adopted in our case study (Sect. 4).

Snow surface albedo:

$$\alpha_{\text{snow}} = 0.82 - 0.03T_a - 1.74 \times 10^{-3}T_a^2 - 1.14 \times 10^{-4}T_a^3 \quad (20)$$

Glacier surface albedo:

$$\alpha_{\text{ice}} = 0.27 - 0.01T_a \quad (21)$$

where T_a is the daily mean air temperature (°C). When it snows the glacier is covered with snow and Eq. (20) can be used to calculate α^g. Otherwise, due to the existence of snow in the accumulation zone of the glacier, average albedo should be weighted according to the snow cover ratio of glacier surface ε_n^g, which could be estimated by experience or calibration.

The long-wave radiation R_{nl}^g depends on ground surface characteristics, air water vapor, clouds, carbon dioxide, and dust condition, and can be estimated as follows (Shuttleworth, 1993; Allen et al., 1998):

$$R_{nl}^g = \sigma \left(\frac{T_{a,\max}^4 + T_{a,\min}^4}{2} \right) \left(0.34 - 0.044\sqrt{e_a} \right) \left(1.35 \frac{R_s^g}{R_{so}^g} - 0.35 \right) \quad (22)$$

where R_{nl}^g is net outgoing long-wave radiation ($\text{MJm}^{-2}\text{day}^{-1}$), σ is Stefan-Boltzmann constant, i.e., 4.903×10^{-9}($\text{MJK}^{-4}\text{m}^{-2}\text{day}^{-1}$), $T_{a,\max}$ is the daily maximum absolute temperature (K), $T_{a,\min}$ is the daily minimum absolute temperature (K), e_a is the actual vapor pressure (kPa), R_s^g is the solar radiation ($\text{MJm}^{-2}\text{day}^{-1}$), and R_{so}^g is clear-sky

radiation ($MJm^{-2}day^{-1}$).

(3) Heat exchange rate with atmosphere (Q^{gT})

Q^{gT} can be divided into two components. One is the energy flux associated with rainfall or snowfall which is denoted by Q_1^{gT}, the other is the sensible heat flux caused by turbulent air motions above the glacier surface, which is denoted by Q_2^{gT}. This is slightly different from Tian et al. (2006a), which includes only the latter term.

$$Q_1^{gT} = \begin{cases} \left(c_{pl}/\rho_l\right) \cdot \left(T_a - \overline{T^g}\right) \cdot e_l^{gT} \text{ for rainfall} \\ \left(c_{pi}/\rho_i\right) \cdot \left(T_a - \overline{T^g}\right) \cdot e_i^{gT} \text{ for snowfall} \end{cases} \quad (23)$$

$$Q_2^{gT} = \omega^g c_{pa} D_h^g \left(T_a - \overline{T^{gs}}\right) \quad (24)$$

where c_{pl},c_{pi},c_{pa} are, respectively, the specific heats of water, ice and air at constant pressure ($kJ/(m^3 \cdot K)$); ρ_l,ρ_i,ρ_a are, respectively, the density of water, ice, and air (kg/m^3); T_a is air temperature (^oC); $\overline{T^{gs}}$ is the glacier surface temperature, which can be replaced by $\overline{T_g}$. D_h^g is the turbulent transfer coefficient estimated using Eqs. (24)–(28) below (Price and Dunne, 1976):

$$D_{hn}^g = \kappa^2 u \Big/ \left[\ln\left((z' - Z - d)/z_0\right)\right]^2, \text{ for neutral condition} \quad (25)$$

$$D_{hs}^g = D_{hn}^g \Big/ \left(1 + 10R_i^g\right), \text{ for stable condition} \quad (26)$$

$$D_{hu}^g = D_{hn}^g \left(1 - 10R_i^g\right), \text{ for unstable condition} \quad (27)$$

HESSD
4, 3627–3686, 2007

EGU

$$R_i^{=} g\,(z' - Z - d) \cdot \frac{\left(T_a - \overline{T^{gs}}\right)}{u^2} \cdot \frac{1}{(T_a + 273.15)} \tag{28}$$

where D^g_{hn},D^g_{hs}, D^g_{hu} are the turbulent transfer coefficient under neutral conditions, stable conditions, and unstable conditions, respectively, κ is von Karman's constant (≈0.40), u is wind speed (m/s) (measured at height z' (m)), Z is depth of glacier and its covers above ground surface (m), d is the zero plane displacement height (m), z_0 is the aerodynamic roughness height over the glacier surface (m), and R_i is the Richardson number.

(4) Glacier surface evaporation (e^g_{lg}) and related latent heat flux ($l'_{lg}e^g_{lg}$)

e^g_{lg} is the combined phase transition term either by evaporation from water or sublimation from ice, which will contribute to the latent heat flux across the glacier surface. Usually it is hard to distinguish between evaporation and sublimation and therefore they can be calculated together.

$$e^g_{lg} = \omega^g \rho_a D^g_h \left[q_s \overline{T^{gs}} - q_a\right] \tag{29}$$

$$l'_{lg} = l_{lg} + l_{ig} - \left(c_{pi}/\rho_i\right) \cdot \overline{T^{gs}} \tag{30}$$

where q_s is the saturation specific humidity of the glacier surface at $\overline{T^{gs}}$ which is replaced by $\overline{T_g}$, q_a is the specific humidity of atmosphere (kg kg^{-1}), l_{lg} and l_{ig} are the latent heats of vaporization and sublimation, respectively (kJ/kg), c_{pi} is the specific heat of ice at constant pressure (kJ/m^3 K), and ρ_a andρ_i are the densities of air and ice (kg/m^3), respectively; the meanings of other symbols are similar to those of Eq. (24).

HESSD
4, 3627–3686, 2007

It should be noted that the above equations for sensible and latent heat flux are point-scale and are subject to the effects of spatial heterogeneity due to the spatial variability of temperature, wind speed, glacier depth. In the interest of simplicity, areal averaged sensible and latent heat flux are replaced by the ones at mean elevation of watershed multiplied by coefficients c_2^{gT} and c_{lg}^{g}, respectively, which is similar to Eq. (16). More sophisticated schemes explicitly accounting for the effects of the actual heterogeneity present could be adopted or developed; this is left for future research.

(5) Melting (e_{il}^{g})

When the total energy supply exceeds the negative heat storage of the g-zone, i.e., $l_{lg}e_{lg}^{g}+l_{ig}e_{ig}^{g}+\overline{R_n^g}\omega^g+Q^{gT}>y^g\omega^g c_{pi}\left(0-\overline{T^g}\right)$, glacier melting will occur and the temperature of g-zone will be kept at zero, i.e., $\overline{T^g} \equiv 0^{\circ}$C. We thus obtain the following equation:

$$-l_{il}e_{il}^{g} - Q^{gt} = \max\left(l'_{lg}e_{lg}^{g} + \overline{R_n^g}\omega^g + Q^{gT}, 0\right) \tag{31}$$

(6) Runoff generation (e^{gt}) and the accompanying heat flux (Q^{gt})

e^{gt} is the water transportation rate from glacier to sub-stream network zone , i.e., runoff. The water storage capacity in the g-zone is ignored and all the melted water is assumed to flow into the t-zone directly.

$$e_l^{gt} = e_{li}^{g} + e_l^{gT} \tag{32}$$

$$Q^{gt} = \left(c_{pl}/\rho_l\right)\cdot\left(\overline{T^t} - \overline{T^g}\right)\cdot e_l^{gt} \tag{33}$$

HESSD
4, 3627–3686, 2007

where $\overline{T^t}$ is the temperature of the t-zone; the meanings of other symbols are similar to those of Eq. (23).

3.2 Degree-day method for closing snow melting and accumulation equations

The energy balance methods discussed in Sect. 3.1 for the g-zone can also be applied to the n-zone without too many changes. The two exceptions are (a) the net solar radiation is different for diverse albedo of the snow surface, and (b) the infiltration of snowmelt water into the u-zone cannot be neglected. However, the data required for this method is not easy to collect, especially in remote regions, due to the broad extension and spatial heterogeneity of snow pack. We therefore propose a more parsimonious approach to close the snow balance equations based on the widely-used but conceptual degree-day method (Finsterwalder and Schunk, 1887). Using the degree-day method we can omit the heat balance equation, and consequently the only independent unknown is $\left(y^n\right)$ and dependent unknowns are $\left(\omega^n, e^{nT}, e_l^{nu}, e_l^{nt}, e_{lg}^n\right)$.

Area fraction of snow zone (ω^n)

ω^n is the area ratio of snow covered zone which can be related to snow water equivalent with the help of the snow cover depletion curve (Luce et al., 1999), which can be expressed as follows:

$$\omega^n = f\left(W_a / W_{a,\max}\right) \tag{34}$$

where W_a is the snow water equivalent of the n-zoneand $W_{a,\max}$ is the maximum snow water equivalent of the n-zone.

The snow depletion curve embodies the snow cover change resulting from snowmelt, and further influences the area of the remaining zones. Here we assume the following principles: when the snow-pack expands, the areas of the b-zone, v-zone, and t-zone will decrease in that order; conversely, when snow pack contracts, the areas of the three zones will increase in the reverse order. Moreover, the area of the r-zone will keep constant whenever the n-zone expands and contracts. The specific

shape of the curve can be determined by snow course observations or by empirical formulae (Luce et al., 1999).

(1) Precipitation (e^{nT})

We assume that snowfall occur over the n-zone and g-zone only. Mass input from atmosphere to snow covered zone can be expressed by the following equation.

$$e^{nT} = e_l^{nT} \times \omega^n + e_n^{nT} \times \left(1 - \omega^n\right) \tag{35}$$

(2) Snow surface evaporation (e_{lg}^n)

e_{lg}^n is the total evaporation rate from snow surface including evaporation and sublimation, which is calculated by the following formula:

$$e_{lg}^n = c_{lg}^n \times E_0 \times \omega^n \tag{36}$$

where E_0 is the evaporation rate obtained from the evaporation pan, c_{lg}^n is the coefficient of snow surface evaporation, which is assumed to be equal to 0.5, as suggested by Lai and Ye (1991).

(3) Infiltration (e_l^{nu})

e_l^{nu} is the mass exchange rate between the n-zone and u-zone, i.e., infiltration. The infiltration process is greatly influenced by soil properties such as soil moisture and soil temperature. The experimental formula developed by Zhao and Gray (1997, 2001) is adopted in this paper to estimate cumulative infiltration (INF), which can then be transformed into infiltration rate (e_l^{nu}):

$$INF = c_{INF} \times \left(S_0^u\right)^{2.92} \times \left(1 - S_l^u\right)^{1.64} \times \left(\frac{273.15 - \overline{T_K^u}}{273.15}\right)^{-0.45} \times t_0^{0.44} \tag{37}$$

where INF is the cumulative infiltration volume (mm), c_{INF} is the coefficient accounting for spatial heterogeneity, $\overline{T_K^u}$ is the initial soil temperature (K), t_0 is the infiltration time (hour), S_0^u is soil surface saturationS_l^u is the initial moisture content including water and ice for the frozen soil, which can be expressed as:

$$S_l^u = \left(\varepsilon_l^u + \varepsilon_i^u\right) / \varepsilon^u \tag{38}$$

where ε^u is the soil porosity of u-zone.

Equation (36) is also applied to estimate the infiltration from the b-zone and v-zone. The difference among different sub-regions lies in the soil surface saturation,S_0^u, which is the area ratio of the surface sub-region to u-zone. For example, for infiltration from snow-pack to the u-zone, S_0^u is defined as $S_0^{nu}=\omega^n/\omega^u$, while for the v-zone and b-zone, the soil surface saturation should be $S_0^{vu}=\omega^v/\omega^u$ and $S_0^{bu}=\omega^b/\omega^u$, respectively.

(4) Snowmelt (e_{nl}^n)

The degree-day equation first proposed by Finsterwalder and Schunk (1887) and widely used is adopted for snowmelt modeling.

$$e_{nl}^n = \omega^n \times a_{nl} \times (T_a - T_0)^{b_{nl}} \tag{39}$$

where ω^n is the area ratio of n-zone, a_{nl} and b_{nl} are the coefficients of snow melting, T_0 is the critical temperature (^{o}C), and T_a is the daily mean temperature ($^\circ$C).

(5) Runoff generation (e^{nt})

The residual term from snowmelt minus infiltration and evaporation will stay in the snowpack until it exceeds the liquid water-holding capacity, estimated from snow density. The density of new snow is proposed to decrease with temperature, while in the case of old snow it is determined by overburden pressure (Anderson, 1976; Jordan,

1991). Besides for short-term calculations, we should also estimate the infiltration rate within the snowpack and the time taken by the melting water to travel through the snowpack to reach the soil surface (Sun et al., 1999).

3.3 Soil freezing and thawing

In the balance equations for the u-zone, i.e., Eqs. (14) and (15), we take the variables $\left(\varepsilon_l^u, \varepsilon_i^u, \overline{T^u}\right)$ as independent unknowns, and assume the area of the u-zone (ω^u) to be constant. The dependent unknowns are, therefore, $\left(e_l^{ub}, e_l^{uv}, e_l^{un}, e_l^{ut}, Q^{ub}, Q^{uv}, Q^{un}, Q^{ut}\right)$, which can be specified either in terms of driving forces (e.g., observation) or by appropriate closure relationships. However, the total number of unknowns exceeds the number of available equations so we should bring in one more new equation.

Owing to the matric and osmotic potentials, unfrozen soil water is maintained in a balanced state with ice. Assuming the existence of balance between water potential and vapor pressure over pure ice surface, the maximum unfrozen-water content model is applied to couple the mass and energy balance equations in the u-zone (Hu et al., 1992, 2006).

$$\varepsilon_l^u = g(\overline{T^u}) = \varepsilon^u \left[\frac{l_{il}\overline{T^u}}{\overline{T^u} + 273.16} + cR\overline{T_K^u}\right]^{-1/B} (g\psi_b)^{1/B} \tag{40}$$

where ε^u is the soil porosity of the u-zone, l_{il} is the latent heat of melting per unit volume (kJ/kg), $\overline{T^u}$ and $\overline{T_k^u}$ are the averaged temperatures of the u-zone in ° and in K, respectively, c is the density of solute in soil, (mol/kg), R is the universal gas constant (8.3143J/mol/K), g is the gravitational acceleration (m/s^2), ψ_b is the air entry value of the soil matrix potential (m), and B is the coefficient related to soil texture.

According to Eq. (40), the change of unfrozen water content with soil temperature can be expressed as a function of soil temperature, i.e., $\frac{d\varepsilon_l^u}{d\overline{T^u}} = f(\overline{T^u})$. As a result, the

mass and heat balance Eqs. (14) and (15) can be deduced as follows:

$$\omega^u y^u c^u \frac{d}{dt}\overline{T^u} = Q^{ub} + Q^{uv} + Q^{un} + Q^{ut} + l_{il}\rho_i y^u \omega^u \frac{d}{dt}\left(\varepsilon_i^u\right) \xrightarrow{\text{Eq. (14)}}$$
$$\omega^u y^u c^u \frac{d}{dt}\overline{T^u} = Q^{ub} + Q^{uv} + Q^{un} + Q^{ut} + l_{il}\left(e_l^{ub} + e_l^{uv} + e_l^{un} + e_l^{ut} - \rho_l y^u \omega^u \frac{d}{dt}\left(\varepsilon_l^u\right)\right)$$
$$\xrightarrow{\frac{d\varepsilon_l^u}{dt}=\frac{d\varepsilon_l^u}{d\overline{T^u}}\frac{d\overline{T^u}}{dt}=f(\overline{T^u})\frac{d\overline{T^u}}{dt}}$$
$$\omega^u y^u c^u \frac{d}{dt}\overline{T^u} = Q^{ub} + Q^{uv} + Q^{un} + Q^{ut} + l_{il}\left(e_l^{ub} + e_l^{uv} + e_l^{un} + e_l^{ut} - \rho_l y^u \omega^u \left(f(\overline{T^u})\frac{d\overline{T^u}}{dt}\right)\right)$$
$$\longrightarrow \omega^u y^u c^u \frac{d}{dt}\overline{T^u} = \omega^u y^u c^u \times \frac{Q^{ub}+Q^{uv}+Q^{un}+Q^{ut}+l_{il}(e_l^{ub}+e_l^{uv}+e_l^{un}+e_l^{ut})}{\omega^u y^u [c^u + l_{il}\rho_l \times f(\overline{T^u})]} \tag{41}$$

$$\frac{d\varepsilon_l^u}{dt} = \frac{d\varepsilon_l^u}{d\overline{T^u}}\frac{d\overline{T^u}}{dt} = f(\overline{T^u})\frac{d\overline{T^u}}{dt} \xrightarrow[\times \rho_l y^u \omega^u]{\text{Eq. (41)}}$$
$$\rho_l y^u \omega^u \frac{d\varepsilon_l^u}{dt} = \rho_l y^u \omega^u f(\overline{T^u}) \frac{Q^{ub}+Q^{uv}+Q^{un}+Q^{ut}+l_{il}(e_l^{ub}+e_l^{uv}+e_l^{un}+e_l^{ut})}{\omega^u y^u [c^u + l_{il}\rho_l \times f(\overline{T^u})]} \tag{42}$$

$$\rho_l y^u \omega^u \frac{d}{dt}\left(\varepsilon_l^u\right) = e_l^{ub} + e_l^{uv} + e_l^{un} + e_l^{ut} - \rho_i y^u \omega^u \frac{d}{dt}\left(\varepsilon_i^u\right)$$
$$\xrightarrow{\text{Eq. (42)}} \rho_i y^u \omega^u \frac{d}{dt}\left(\varepsilon_i^u\right) =$$
$$e_l^{ub} + e_l^{uv} + e_l^{un} + e_l^{ut} - \rho_l y^u \omega^u f(\overline{T^u}) \frac{Q^{ub}+Q^{uv}+Q^{un}+Q^{ut}+l_{il}(e_l^{ub}+e_l^{uv}+e_l^{un}+e_l^{ut})}{\omega^u y^u [c^u + l_{il}\rho_l \times f(\overline{T^u})]} \tag{43}$$

(1) Infiltration/exfiltration (e_l^{uv}, e_l^{ub}, and e_l^{un})

From a hydrological point, e_l^{uv}, e_l^{ub}, e_l^{un} are infiltration or exfiltration terms between the u-zone and the v-zone, b-zone, and n-zone, respectively, which can be calculated using equations similar to Eqs. (37) and (38).

(2) Heat exchange rate above sub-regions (Q_l^{uv}, Q_l^{ub}, and Q_l^{un})

Q_l^{uv}, Q_l^{ub} , and Q_l^{un} are the heat exchanges between the u-zone and the v-zone, b-zone, and n-zone, respectively, which include the heat fluxes associated with infiltration/exfiltration, and the heat conduction terms between them. Take vegetation zone for example; the heat exchange rate is calculated by the following equation:

$$Q^{uv} = -Q^{vu} = -\left(c_{pl}/\rho_l\right) \cdot e_l^{vu} \cdot \left(\overline{T^u} - \overline{T^v}\right) + \overline{D^u}\omega^v \left(\overline{T^v} - \overline{T^u}\right) \cdot \left(0.5\left(y^v + y^u\right)\right) \quad (44)$$

where the first term on r.h.s. represents heat flux associated with mass exchange, the second one accounts for heat conduction, c_{pl} is the specific heat of water at constant pressure (kJ/(m^3·K)), and $\overline{D^u}$ is the averaged coefficient of thermal conductivity (kW/(m·K)).

(3) Runoff generation (e_l^{ut}) and the accompanying heat flux (Q_l^{ut})

e_l^{ut} is the saturation excess runoff which can be calculated as follows.

$$e_l^{ut} = \begin{cases} 0 & \varepsilon_l^u + \varepsilon_i^u \le \varepsilon_c^u \\ \Delta w & \varepsilon_l^u + \varepsilon_i^u > \varepsilon_c^u \end{cases} \quad \text{where} \quad \Delta w = -(e_l^{uv} + e_l^{ub} + e_l^{un}) \quad (45)$$

where ε_c^u is the soil moisture at field capacity.

The accompanying heat flux can be calculated using:

$$Q^{ut} = \left(c_l^u/\rho_l^u\right) \cdot e_l^{ut} \cdot \left(\overline{T^t} - \overline{T^u}\right) \quad (46)$$

4 Application to the headwaters of the Urumqi River

4.1 Study area: headwaters of the Urumqi River

The development and testing of the constitutive relationships are performed at the headwaters of the Urumqi River (see Fig. 4). The Urumqi River is located within the Tianshan Mountain, in the north-west of China, and originates from Peak Tianger II, located at an elevation of 4486 m, and flows northward to Urumqi City of China. The

headwaters of the river are situated in a permafrost region, seasonally covered by snow, and drain an area of 28.9 km^2 with an average elevation of 3860 m. It contains 7 glaciers with a total area of 5.6 km^2, of which the biggest one is No. 1 Glacier with an area of 1.84 km^2.

The headwaters of the Urumqi River are one of the most heavily instrumented and well studied experimental watersheds in the cold regions of China. There are 3 streamflow gauging stations, i.e., Total Control station (the outlet station), No. 1 Glacier station, and Kongbingdou station, and 1 meteorological/ weather station named Daxigou located at the elevation of 3539 m, and many other routine observations of glacier mass and energy balance, glacier movement, and frozen hydrologic issues conducted over many years by different researchers (Yang et al., 2000; Shi et al., 2000).

Runoff in the Urumqi River is contributed from precipitation as well as glacier melt and snowmelt. According to Daxigou meteorological station and the Total Control hydrological station, the mean annual precipitation is about 400mm, of which over 75% happens during the summer season from May to August. Mean air temperature during the summer season is about 3^{o}C which leads to melting of glacier and snow pack (see Fig. 5 for the mean monthly precipitation and positive accumulated air temperature). It is reported that runoff volume during the summer season comprised 90% of yearly runoff volume (Yang and Han, 1994). Our case study will focus on the runoff modeling during summer season.

4.2 Data pre-processing

(1) Air temperature

Air temperature decreases with elevation at rate of −0.68°/100 m in the headwaters of the Urumqi River according to Ding et al. (1998). We transform the air temperature at Daxigou meteorological station to average air temperature at mean elevation of the study area.

(2) Ground surface temperature

The temperature of the t-zone, b-zone, and v-zone are assumed to be equal, and denoted as ground surface temperature. The MODIS images of the watershed in 2002 are used to derive the relationship between daily mean air temperature and temperature difference between air and ground surface, as shown in Fig. 6. The temperature measured by remote sensing image is always at some specific time, e.g. 10:30 a.m. (local time) for the image shown in Fig. 6, which should be transformed to the daily mean temperature with the help of a correspondence curve relating the point value and the daily mean value.

(3) Precipitation

The precipitation data cannot be used until error corrections are made for use in mountainous regions (Yang et al., 1988). The type of precipitation depends on the air temperature, which can be expressed as follows:

$$\begin{cases} T \geq T_1 & \text{rain}=P & \text{snow}=0 \\ T_1 > T \geq T_2 & \text{rain}=P \times k_1 & \text{snow}=P \times (1-k_1) \\ T < T_2 & \text{rain}=0 & \text{snow}=P \end{cases} \quad (47)$$

According to Kang and Ohmura (1994), the critical temperature T_1, T_2 for Daxigou meteorological station are 5.5°C and 2.8°C, respectively. The temperature data is, however, the average one at mean elevation of the watershed as mentioned above, and therefore both critical temperatures should be subjected to some calibration.

(4) Snow depletion curve

The snow cover depletion curve is expressed as (Luce and Tarboton, 2004):

$$\omega^n = F\left(W_a / W_{a,\max}\right) \quad (48)$$

where ω^n is the area ratio of snow covered zone, W_a is snow water equivalent $W_{a,\max}$ is the maximum snow water equivalent of the watershed, F is a function of the snow

cover depletion curve, whose form also needs to be calibrated. Here we adopt the snow cover depletion curve (see Eq. 49) obtained by Luce et al. (1999) in Upper Sheep Creek, a sub-watershed of the Reynolds Creek Experimental Watershed in south-western Idaho. The shape of the snow cover depletion curve is not as critical in our case study due to the smaller influence of snow melt as compared to glacier melt on runoff generation.

$$\omega^n = \begin{cases} 0.18\sqrt{W_a/W_{a,\max}} & 0 \le W_a/W_{a,\max} \le 0.13 \\ 0.42\sqrt{W_a/W_{a,\max} - 0.11} & 0.13 \le W_a/W_{a,\max} \le 0.34 \\ \left(W_a/W_{a,\max}\right)^{1.5} & 0.34 \le W_a/W_{a,\max} \le 1 \end{cases} \quad (49)$$

4.3 Model calibration

The Urumqi River is an ephemeral stream which runs dry from late September to the following April. In this paper we focus on the runoff simulation from May to August only. The 6-year period from 1990 to 1995 is chosen for model calibration and validation, while excluding 1992 due to inadequate and abnormal data (See Fig. 7, for example, the discharge is quite different during the two days identified by two dotted lines, but with similar air temperatures; the gauged streamflow increased when air temperature decreased in the left circle, while the opposite trend happens in the right circle). The calibration period is 1990–1994 excluding 1992, and the validation period is 1995. The main climatic characteristics during the period of model application are listed in Table 2.

In Sect. 3 we proposed two different closure schemes for g-zone and n-zone. In our case study, the energy balance method (Sect. 3.1) is adopted for the g-zone and the degree-day method (Sect. 3.2) is adopted for the n-zone. We use a single REW for the whole study area (28.9 km^2) while allowing the spatial heterogeneity inherent in the various hydrological processes to be represented by the corresponding parameters in the closure relationships.

The geographic data such as drainage area, slope, channel length etc. are extracted

HESSD
4, 3627–3686, 2007

from a DEM with 25 m×25 m resolution (Table 3). The main types of landscape are glacier, snow, swamp, gravel desert, and high mountainous meadow. The soil types underlying the study area include cold desert soils, alpine meadow soil and peat bog soil (Kang et al., 1997).

The parameters subject to calibration are listed in Table 5. We represent the seasonal frozen layer with initial soil ice contents instead of layer depths. The initial soil ice content of each year is determined by the mean daily maximum air temperature from January to April (see Fig. 8). Three standard indices, i.e., Nash-Sutcliffe efficiency coefficient, water balance index, and relative error, are selected to guide model calibration, see Eqs. (50)–(52). The evaluation metrics and the calibrated results are shown in Table 6, and Figs. 9 to 13.

Nash-Sutcliffe efficiency coefficient:

$$R^2 = 1 - \frac{S^2}{\sigma^2} \quad S = \sqrt{\frac{\sum_{i=1}^{n}(Q_{oi} - Q_{si})^2}{n}} \quad \sigma = \sqrt{\frac{\sum_{i=1}^{n}(Q_{oi} - \overline{Q_{oi}})^2}{n}} \tag{50}$$

Water balance index : $$IVF = \sum Q_{si} / \sum Q_{oi} - 1 \tag{51}$$

Relative error : $$R_E = \frac{1}{n\overline{Q_{oi}}} \sum_{i=1}^{n} |Q_{oi} - Q_{si}| \tag{52}$$

where Q_{oi}, Q_{si} are observed and simulated daily discharges, respectively, n is the total number of time steps.

During the four year calibration period, we obtained an R^2 value falling within 0.64~0.80, IVF within -0.12~0.073, and R_E within 0.24~0.34. The highest R^2 and

the lowest IVF and R_E are obtained simultaneously in the dry and warm year (1990, see Table 6 and Table 2). This may due to the fact that glacier melting is the dominant process in the study area, which will be explained later. From Fig. 9 we can see that the total runoff is influenced by water input as well as energy input, as indicated by air temperature. When there is rainfall the discharge jumps quickly due to the small catchment area and hence short residence time, but when there is no significant rainfall the hydrograph is mainly determined by the variation of air temperature and the discharge increases or decreases not sharply but gradually. Figure 10 shows the correlation between observed discharge and the simulated one via a 1:1 straight line, and we can see that there is no significant systematic deviation for different flow regimes, e.g. high flow regime and low flow regime. The daily water depths of snow and glacier melting and precipitation over the whole catchment are illustrated in Fig. 11, which shows that the glacier melting is much more important than snowmelt and precipitation, especially after July. This should be attributable to the large area ratio covered by glacier in the study catchment, as well as the warm weather condition during summer. Similarly, snow water equivalent experiences a dramatic drop and soil water content experiences a steady increase after July, as demonstrated in Fig. 12 and Fig. 13, respectively. Figure 13 also demonstrates the decreasing trend of soil ice content during the melting season and the roughly similar pattern of soil water and ice dynamics in different years.

4.4 Model validation

Using the parameters obtained by calibration over the period 1990–1994, the model is then validated for the year 1995. The results are shown in Table 6 and Fig. 14 from which similar conclusions can be drawn from the validation period as from the calibration period (Sect. 4.3).

Sensitivity analysis of the model during calibration and validation periods shows that the water balance index (IVF) is least sensitive at the daily time step and moderate runoff while all three indices (R^2, IVF, and R_E) are highly sensitive to the initial condition, i.e., initial soil ice content, on which the Nash-Sutcliffe efficiency is most sensitive.

This is due to the short calibration period during which the effects of initial conditions could not be eliminated.

5 Summary and conclusion

As stated by many researchers (Beven, 2002, 2006; Zehe and Sivapalan, 2007; Reggiani and Schellekens, 2003; Lee et al., 2007), the closure problem is one of the most crucial issues standing in the way of the REW approach becoming an alternative blueprint for distributed hydrological modeling. Although great progress has been made in theoretical and applied aspects of the REW approach in recent years (Reggiani et al., 1998, 1999; Reggiani and Rientjes, 2005; Tian et al., 2006a, b; 2007; Lee et al., 2007; Zhang et al., 2006), energy balance equations have been excluded in these applications. The development and testing of appropriate constitutive relationships for processes occurring in cold regions continue to hamper its application to cold and even temperate regions.

In this paper, within the extended framework of the REW approach provided by Tian et al. (2006a), we proposed a set of closure schemes for cold region processes. These were classified into two different types, i.e., melting and accumulation of glacier/snow, and freezing and thawing of soil water. A rigorous energy balance method has been proposed to close the balance equations of melting/accumulation processes, along with the conceptual degree-day method. The closure schemes for soil freezing and thawing are based on the maximum unfrozen-water content model. We applied the proposed closure schemes to the headwaters of the Urumqi River and obtained very promising results. The modeling shows

It should be noted that the constitutive relationships proposed in this paper are specified for cold regions processes, which may not occur throughout the year in all cold regions. For example, in seasonally frozen areas soil may behaves as frozen soil in the cold season and as normal soil in the warm season, and for seasonally snow-covered areas, snow cover accumulates during the cold season and melts and disappears dur-

ing the warm season. The simulation of the switching pattern can be accomplished by switching the closure schemes in different seasons, in which case the transition between accumulation and melting should be modeled very carefully.

In our case study, the runoff contributed by glacier melting turned out to be the most important component, and for this reason in this paper we focused on the melt processes of glacier and deal with the other processes in a relatively simpler manner. Although the closure schemes developed in this paper will not prevent us to focus on snow melt processes, more detailed analyses should be carried out to investigate snow accumulation and redistribution, and the depletion for snow cover will become dominant in most cold catchments. These difficult issues and the generalization of the REW framework to deal with these are left for future research.

Nomenclature

Latin symbols

a_{nl}	Coefficient of daily snow melting	
a_s	Regression constant	
b_{nl}	Coefficient of daily snow melting	
b_s	Regression constant	
B	Coefficient of unfrozen water content model related to soil texture	
c	Density of solute in soil	$[\mathrm{molM}^{-1}]$
c_{INF}	Coefficient of infiltration	
c_{rn}^{g}	Coefficient of radiation of g-zone	
c_{2}^{gT}	Coefficient of sensible heat flux of g-zone	
c_{lg}^{g}	Coefficient of latent heat flux of g-zone	
c_{lg}^{n}	Coefficient of snow surface evaporation	
c_n	Coefficient of unit transformation from $[\mathrm{MJm}^{-2}\mathrm{day}^{-1}]$ to $[\mathrm{kWm}^{-2}]$	

HESSD
4, 3627–3686, 2007

$c_{pl}c_{pi}c_{pa}$	Specific heat of water, ice and air at a constant pressure	$\left[ML^{-1}T^{-2}\Theta^{-1}\right]$
c^u	Averaged specific heat of u-zone	$\left[ML^{-1}T^{-2}\Theta^{-1}\right]$
d_r	Zero plane displacement	$[L]$
d_r	Inverse relative distance Earth-Sun	
$D_h^g, D_{hn}^g, D_{hs}^g, D_{hu}^g$	Turbulent transfer coefficient and its special form under neutral, stable and unstable conditions respectively	
$\overline{D^u}$	Averaged coefficient of thermal conductivity	$\left[MLT^{-3}\Theta^{-1}\right]$
e_a	Actual vapor pressure	$\left[ML^{-1}T^2\right]$
E_0	Evaporation rate obtained from evaporation pan	$\left[LT^{-1}\right]$
F	The function of snow cover depletion	
g	Gravitational constant	$\left[LT^{-2}\right]$
INF	Cumulative infiltration volume	$[L]$
IVF	Water balance index	
k_1	Rain ratio when rain and snow happen together	
$\overline{K_s^s K_s^u}$	Hydraulic conductivity in s-zone and u-zone respectively	$\left[LT^{-1}\right]$
l_{lg}, l_{il}, l_{ig}	Latent heat of vaporization, melting, and sublimation	$\left[L^2T^{-2}\right]$
l^r	Channel length	$[L]$
m^r	Cross-section area of main channel	$\left[L^2\right]$
n^r, n^t	Manning's n (r-zone), Manning's n (t-zone)	
n	Total time steps of observed or simulated daily discharge	

HESSD
4, 3627–3686, 2007

n_{sun}	Actual duration of sunshine	$[T]$
N_{sun}	Maximum possible duration of sunshine or daylight hours	$[T]$
P	The quantity of daily precipitation	$[L]$
q_a, q_s	Actual humidity and saturated humidity	
Q^{gT}	Heat exchange rate with atmosphere of g-zone	$\left[ML^2T^{-3}\right]$
Q_1^{gT}	Energy flux of g-zone accompanied with rainfall or snowfall	$\left[ML^2T^{-3}\right]$
Q_2^{gT}	Sensible heat flux of g-zone	$\left[ML^2T^{-3}\right]$
Q_{oi}, Q_{si}	Observed or simulated daily discharge at the ith step respectively	$\left[LT^{-3}\right]$
rain	The quantity of daily rainfall	$[L]$
R^2	Nash -Sutcliffe efficiency coefficient	
R_E	relative error,	
R_i	Richardson number	
R_a	Daily extraterrestrial radiation	$\left[MT^{-3}\right]$
R_{so}^g	Clear-sky radiation of g-zone	$\left[MT^{-3}\right]$
R_s^g	Local surface solar radiation	$\left[MT^{-3}\right]$
R_{nl}^g	Local net long-wave radiation	$\left[MT^{-3}\right]$
$\overline{R_n^g}$	Areal averaged net radiation intensity	$\left[MT^{-3}\right]$
snow	The quantity of daily snowfall	$[L]$
$S_0^u, S_0^{nu}, S_0^{vu}, S_0^{bu}$	Soil surface saturation and its special form for infiltration from n-zone, v-zone and b-zone respectively.	

HESSD

4, 3627–3686, 2007

S_l^u	Initial moisture content	
t_0	Infiltration time	$[T]$
T_0	Critical temperature of snow melting	$[\Theta]$
T_1	Critical temperature of defining rain form	$[\Theta]$
T_2	Critical temperature of defining snow form	$[\Theta]$
T_a	Daily mean air temperature	$[\Theta]$
$T_{a,\max}$	Daily maximum absolute temperature	$[\Theta]$
$T_{a,\min}$	Daily minimum absolute temperature	$[\Theta]$
$\overline{T^{gs}}$	Glacier surface temperature	$[\Theta]$
$\overline{T^u}$, $\overline{T_K^u}$	Averaged temperature of u-zone in degrees Celsius, Kelvin respectively	$[\Theta]$
u	Wind speed	$\left[LT^{-1}\right]$
w^r	Channel width	$[L]$
W_a	Snow water equivalent of n-zone	$[L]$
$W_{a,\max}$	Maximum snow water equivalent of n-zone	$[L]$
y^j	Depth of j-zone	$[L]$
Z	Depth of glacier and its covers (above ground surface)	$[L]$
z'	Height of measured wind speed	$[L]$

Greek symbols

α^g	Albedo of glacier surface	
α_{ice}, α_{snow}	Ice and snow surface albedo	
ε_n^g	Snow ratio of glacier surface	
ε_l^u, ε_i^u	Soil liquid water content, ice content respectively.	
ε_c^u	Soil field moisture capacity.	
$\varepsilon^u \varepsilon^s$	Soil porosity of u-zone and s-zone respectively	
$\overline{\rho_\alpha^j}$	the time-averaged density of B_α^j	$\left[ML^{-3}\right]$

ρ_α^j	the density of α phase at the differential volume dV in V_α^j space	$\left[ML^{-3}\right]$
φ	Latitude	
φ_b	Soil matrix potential of air entry	$[L]$
σ	Stefan-Boltzmann constant	$\left[MT^{-3}\Theta^{-4}\right]$
μ	Soil pore distribution index	
κ	Von Karman's constant	
δ	Solar declination	
Σ	Horizontal projected Area of watershed	$\left[L^2\right]$
γ^r, γ^t	Slope of r-zone Slope of t-zone	
ω_s	Sunset hour angle	
ω^j	Time-averaged horizontal projected area ratio of j-zone	

Subscripts and superscripts

B	superscript indicating the impermeable strata or groundwater reservoir
EXT	superscript indicating the external world
i, j	superscripts indicating sub-region, can be u(unsaturated zone), s(saturated zone), r(main channel reach), t(sub-stream network), b(bared soil zone), v(vegetation covered zone), n(snow covered zone), g(glacier covered zone)
L	superscript indicating the neighboring REW, $L = 1..N_K$
P	superscript indicating the wildcard indicating $EXT, L, T, B, i, L = 1..N_K$
T	superscript indicating the atmosphere
α, β	subscripts indicating the phase, can be m (soil matrix), l (liquid water), a (gaseous phase), p (vapor), i (ice), n (snow), and v (vegetation)

Note: M is the dimension of mass, L is the dimension of length, T is the dimension of time, and Θ is the dimension of temperature. mol is the dimension of mol.

Acknowledgements. We appreciate the valuable instructions and suggestions of Professor Ye Bosheng, and also acknowledge Dr. Han Tianding for access to the data used in this paper. This research was supported by the project "Study of the theory and application of hydrological simulations based on the representative elementary watershed" (50509013) sponsored by the National Natural Science Foundation of China (NSFC).

References

Abbott, M. B., Bathurst, J. C., and Cunge, J. A.: Intruction to the European hydrological system – Systeme Hydrologique Europeen, "SHE", 1: History and philosophy of a physically-based, distributed modelling system, J. Hydrol., 87(1–2), 45–59, 1986a.

Abbott, M. B., Bathurst, J. C., and Cunge, J. A.: Intruction to the European hydrological system – Systeme Hydrologique Europeen, "SHE", 2: Structure of a physically-based, distributed modelling system, J. Hydrol., 87(1–2), 61–77, 1986b.

Allen, R. G., Pereira, L. S., Raes, D., and Smith, M. (Eds): Crop evapotranspiration: Guidelines for computing crop water requirements, FAO, Rome, 1998.

Anderson, E.: A point energy and mass balance model of a snow cover., Office of Hydrology, National Weather Service, Silver Spring, Maryland, NOAA Technical Report NWS 19,1976.

Beven, K.: Searching for the Holy Grail of scientific hydrology: $Q_t = H(A)$ as closure, Hydrol. Earth Syst. Sci., 10, 609–618, 2006, http://www.hydrol-earth-syst-sci.net/10/609/2006/.

Beven, K.: Towards an alternative blueprint for a physically based digitally simulated hydrologic response modelling system, Hydrol. Process., 16(2), 189–206, 2002.

Cohen, S. D. and Hindmarsh, A. C.: CVODE, a stiff/nonstiff ODE Solver in C, Comput. Phys., 10(2), 138–143, 1996.

Coleman, B. D. and Noll, W.: The thermodynamics of elastic materials with heat conduction and viscosity, Arch. Ration. Mech. Analysis., 13, 168–178, 1963.

Cross, H.: Analysis of Flow in Networks of Conduits or Conductor, University of Illinois Bulletin, 286, 3–32, 1936.

Ding, Y. J., Li, X., and Cheng, G. D.: Potential Direct Solar Radiation Based on GIS and Glacier Mass Balance, J. Glaciol. Geocryol., 20(2), 12–17, 1998.
Finsterwalder, S. and Schunk, H.: Der Suldenferner., Zeit schrift des Deut schen und Oesterreichischen Alpenvereins, 18, 72–89, 1887.
Freeze, R. A. and Harlan, R. L.: Blueprint for a physically-based,digitally-simulated hydrologic response model, J. Hydrol., 9(3), 237–258, 1969.
Gray, D. M., Toth, B., Zhao, L. T., Pomeroy, J. W., and Granger, R. J.: Estimating areal snowmelt infiltration into frozen soils, Hydrol. Process., 15, 3095–3111, 2001.
Hu, H. P., Yang, S. X., and Lei, Z. D.: A numerical simulation for heat and moisture transfer during soil freezing, J. Hydrol. Eng., 7(6), 1–8, 1992.
Hu, H. P., Ye, B. S., Zhou, Y. H., and Tian, F. Q.: A Land Surface Model Incorporated with Soil Freeze/Thaw and Its Application in GAME/Tibet, Science in China, Ser. D, 36(7), 755–766, 2006.
Jordan, R.: A one-dimensional temperature model for a snow cover, US Army Corps of Engineers. Cold Regions Research and Engineering Laboratory, 1991.
Kang, E. S. and Ohmura, A.: Water, heat balance and runoff model in the source area of Urumqi River in the Tianshan Mountains., Science in China, Ser. B, 24(8), 983–991, 1994.
Kang, E. S., Shi, Y. F., Yang, D. Q., Zhang, Y. S., and Zhang, G. W.: An experimental study on runoff formation in the mountianous basin of the Urumqi River, Quaternary Sciences, 2, 140–146, 1997.
Kang, E. S, Yang, D. Q., and Zhang, Y. S.: An experimental study of the water and heat balance in the source area of the Urumqi River in the Tianshan mountains, Ann. Glaciol., 16, 55–56, 1992.
Lai, Z. M. and Ye, B. S.: Water balance model in high cold mountain watershed and runoff change with globe warming-take Urumqi River in Tianshan for example, Science in China, Ser. B, 21(5), 652–658, 1991.
Lalit, K., Andrew, K. S., and Knowles, E.: Modeling topographic variation in solar radiation in a GIS Environment, Int. J. Geogr. Inf. Sci., 11(5), 475–497, 1997.
Lee, H., Sivapalan, M., and Zehe, E.: Representative Elementary Watershed (REW) approach, a new blueprint for distributed hydrologic modeling at the catchment scale: the development of closure relations, Ottawa,Canada, Canadian Water Resources Association (CWRA), 165-218, 2005.
Lee, H., Zehe, E., and Sivapalan, M.: Predictions of rainfall-runoff response and soil moisture

dynamics in a microscale catchment using the CREW model, Hydrol. Earth Syst. Sci., 11, 819–849, 2007, http://www.hydrol-earth-syst-sci.net/11/819/2007/.
Lin, F. T.: Determination and evaluation of water supply source for permafrost areas in Da Hinggan Mountains and Xiao Hinggan Mountains, J. Glaciol. Geocryol., 2(1), 32–36, 1980.
Luce, C. H. and Tarboton, D. G.: The application of depletion curves for parameterization for subgrid variability of snow, Hydrol. Process., 18, 1409–1422, 2004.
Luce, C. H., Tarboton, D. G., and Cooley, K. R.: Sub-grid parameterization of snow distribution for an energy and mass balance snow cover model, Hydrol. Process., 13, 1921–1933, 1999.
McDonnell, J. J., Sivapalan, M., Vaché, K., Dunn, S., Grant, G., Haggerty, R., Hinz C., Hooper R., Kirchner, K., Roderick, M. L., Selker, J., and Weiler, M.: Moving beyond descriptions of watershed heterogeneity and process complexity: A new vision for watershed hydrology, Water Resour. Res., in press, 2007.
McManamon, A., Day, G., and Carroll, T.: Snow estimation - A gis application for water resources forcasting, in: Proceedings of the Symposium on Engineering Hydrology, ASCE Publ., New York, 856–861, 1993.
Ni, G. H., Liu, Z. Y., Lei, Z. D., Yang, D. W., and Wang, L.: Continuous Simulation of Water and Soil Erosion in a Small Watershed of the Loess Plateau with a Distributed Model, J. Hydraul. Eng.-ASCE, in press, 2007.
Price, A. D. and Dunne, T.: Energy balance computations of snow melt in a sub-arctic area, Water Resour. Res., 12, 686–689, 1976.
Reggiani, P. and Schellekens, J.: Modelling of hydrological responses: the representative elementary watershed approach as an alternative blueprint for watershed modelling, Hydrol. Process., 17, 3785–3789, 2003.
Reggiani, P. and Rientjes, T. H. M.: Flux parameterization in the Representative Elementary Watershed (REW) Approach: application to a natural basin, Water Resour. Res., W04013, 1–8, 2005.
Reggiani, P., Sivapalan, M., and Hassanizadeh, S. M.: Conservation equations governing hillslope responses, Water Resour. Res., 38(6), 1845–1863, 2000.
Reggiani, P., Sivapalan, M., and Hassanizadeh, S. M.: Unifying framework for watershed thermodynamics: balance equations for mass, momentum, energy and entropy, and the second law of thermodynamics, Adv. Water Resour., 22(4), 367–398, 1998.
Reggiani, P., Sivapalan, M., and Hassanizadeh, S. M.: Unifying framework for watershed ther-

modynamics: constitutive relationships, Adv. Water Resour., 23(1), 15–39, 1999.
Reggiani, P., Sivapalan, M., Hassanizadeh, S. M., and Gray, W. G.: Coupled equations for mass and momentum balance in a stream network: theoretical derivation and computational experiments, Proc. Roy. Soc. Lond, 457, 157–189, 2001.
Shi, Y. F., Huang, M. H., and Yao, T. D. (Eds): Glaciers and their environments in China-the present, past, and future, Science Press, Beijing, China, 2000.
Shuttleworth, W. J.: Evaporation, in: Handbook of Hydrology, Maidment, D.R., McGraw-Hill, New York., 4.1–4.53, 1993.
Sivapalan, M.: Prediction in ungauged basins: a grand challenge for theoretical hydrology, Hydrol. Process., 17, 3163–3170, 2003a.
Sivapalan, M., Takeuchi, K., Franks, S. W., Gupta, V. K., Karambiri, H., Lakshmi, V., Liang, X., McDonnell, J. J., Mendiondo, E. M., O'Connel, P. E., Oki, T., Pomeroy, J. W., Schertzer, D., Uhlenbrook, S., and Zehe, E.: IAHS decade on Predictions of Ungauged Basins (PUB): Shaping an exciting future for the hydrological sciences, Hydrol. Sci. J., 48(5), 857–879, 2003b.
Sun, S. F., Jin, J., and Xue, Y. K.: A simple snow-atmosphere-soil transfer model, J. Geophys. Res., 104(D16), 19 587–19 587, 1999.
Taibi, A. E. O., Zhang, G. P., and Elfeki, A.: Hydrologic responses of the Zwalm catchment using the REW model: incorporating uncertainty of soil properties, Hydrol. Earth Syst. Sci. Discuss, 3, 69–114, 2006.
Tian, F. Q., Hu, H. P., Lei, Z. D., and Sivapalan, M.: Extension of the representative elementary watershed approach for cold regions via explicit treatment of energy related processes, Hydrol. Earth Syst. Sci., 10, 619–644, 2006a.
Tian, F. Q.: Study on Thermodynamic watershed hydrological model (THModel). Ph. D. thesis, Tsinghua University, China, 2006b.
Tian, F. Q., Hu, H. P., and Lei, Z. D.: Thermodynamic watershed hydrological model: constitutive relationship., Science in China, Ser. E, in press, 2007.
Williams, K. S. and Tarboton, D. G.: The ABC's of snowmelt: a topographically factorized energy component snowmelt model, Hydrol. Process., 13, 1905–1920, 1999.
Yang, D. Q., Jiang, T., Zhang, Y. S., and Kang, E. S.: Analysis and Correction of Errors in PrecipitationMeasurement at the Head of UrumqiRiver,Tianshan, J. Glaciol. Geocryol., 10(4), 384–400, 1988.
Yang, X. Y. and Han, T. D.: Climatic Characteristic and Glacial Runoff in the Source of Urumqi

River, J. Glaciol. Geocryol., 16(2), 147–154, 1994.
Yang, Z. N., Liu, X. R., and Zeng, Q. Z. (Eds): Hydrology in cold regions of China, Science Press, Beijing, China, 2000.
Zehe, E., Maurer, T., Ihringer, J., and Plate, E.: Modeling water flow and mass transport in a Loess catchment, Phys. Chem. Earth (B), 26(7–8), 487–507, 2001.
Zehe, E. and Sivapalan, M.: Towards a new generation of hydrological process models for meso-scale: an introduction, Hydrol. Earth Syst. Sci., Special Issue: Towards a new generation of hydrological process models for meso-scale, 1-7, 2007.
Zhang, G. P.: Modeling runoff generation in the Geer river basin with improved model parameterizations to the REW approach, Phys. Chem. Earth, 30(4–5), 285–296, 2005a.
Zhang, G. P. and Savenije, H. H. G.: Rainfall-runoff modeling in a catchment with a complex groundwater flow system: application of the Representative Elementary Watershed (REW) approach, Hydrol. Earth Syst. Sci., 9, 243–261, 2005b.
Zhang, G. P., Savenije, H. H. G., and Fenicia, F.: Modelling subsurface storm flow with the Representative Elementary Watershed (REW) approach: application to the Alzette River Basin, Hydrol. Earth Syst. Sci., 11, 937–955, 2006, http://www.hydrol-earth-syst-sci.net/11/937/2006/.
Zhao, L. T. and Gray, D. M.: A parametric expression for estimating infiltration, Hydrol. Process., 11, 1761–1775, 1997.

Table 1. Principle closure formulae in THModel (Tian et al., 2007; Lee et al., 2007).

No.	Variable	Note	Constitutive relationship
1	ω^t	Area ratio of sub-stream network zone	$\omega^t = \begin{cases} 0 if\ y^s \le z^r - z^s \\ \frac{1}{\beta_1^{\omega^t} + \beta_2^{\omega^t} e^{-\beta_3^{\omega^t}(y^s - Z + \lvert\psi_b\rvert)}} - \frac{1}{\beta_1^{\omega^t} + \beta_2^{\omega^t} e^{-\beta_3^{\omega^t}(z^r - z^s - Z + \lvert\psi_b\rvert)}} & if\ z^r - z^s < y^s < Z \\ 1 if\ y^s = Z \end{cases}$
2	e^{bu}, e^{vu}	infiltration	$F^j = \min\left[R\omega^j,\ \overline{f_i}\omega^j\right], j = b, v \overline{f_i} = \overline{K_s^u}\left[1 + \alpha^{IFL}\frac{\lvert\psi\rvert(1-s^u)\varepsilon^u}{s^u y^u}\right]$
3	e_{lg}^b, e_{lg}^v	Evaporation or transpiration	$ET^j = \min\left\{\left[(1-M)E_p + M(ET_v)\right]\omega^j,\ \overline{f_e}\omega^j\right\}, j = b, v$ $\overline{f_e} = \alpha^{EFL}\frac{\overline{K_s^u}}{(1-s^u)y^u}\frac{(s^u)^{2+d}\varepsilon^u\lvert\psi_b\rvert}{\mu}$
4	e^{us}	Deep seepage or phreatic evaporation	$e^{us} = \alpha^{us}\varepsilon^u\omega^u v_z^u$
5	e^{tr}	Runoff from t-zone	$e^{tr} = \alpha^{tr}\xi^r y^t v^t$
6	e^{st}	Seepage from s-zone	$e^{st} = \omega^t \alpha_1^{st}\overline{K_s^s}^{\alpha_2^{st}}\left[\frac{y^u s^u \omega^u + y^s \omega^s}{(y^u + y^s)\lvert\psi\rvert}\right]^{\alpha_3^{st}}$
7	ψ	Averaged soil matrix potential of u-zone	$\overline{\psi^u} = \psi_b s^{-\alpha}$ α defined by soil characteristic
8	K	Averaged soil hydraulic conductivity of u-zone	$\overline{K^u} = \overline{K_s^u}s^\beta$, β defined by soil characteristic

HESSD
4, 3627–3686, 2007

Table 2. Total precipitation and mean temperature from May to August for 1990–1995 (excluding 1992).

Year	precipitation (mm)	Daily mean temperature(˚C)	Notes
1990	307.3	3.31	Dry, warm
1991	373.4	2.75	Wetter, warmer
1993	401.8	1.98	wet, cold
1994	435.3	3.10	wet, warm
1995	315.1	3.00	dry, warm

Table 3. Physical parameters for THModel in cold regions.

Symbol	Value	Unit	Symbol	Value	Unit
Σ	28.44	(km^2)	n^r	0.03	
ω^t	0.01		n^t	0.05	
ω^g	0.2		$\overline{K_s^u}$	3×10^{-7}	(m/s)
ω^v	0.3		$\overline{K_s^s}$	3×10^{-7}	(m/s)
l^r	3000.3	(m)	ε^u	0.55	
w^r	7	(m)	ε^s	0.55	
γ^r	8.61	(°)	μ	0.25	
γ^t	43.35	(°)	ψ_b	–0.55	(m)

HESSD
4, 3627–3686, 2007

Table 4. Initial conditions for case study in headwaters of Urumqi River basin.

Symbol	Value	Unit
y^n	0.75	(m)
y^g	40	(m)
y^s	6	(m)
y^t	0	(m)
m^r	0.1	(m^2)
y^u	2	(m)
$\overline{T^u}$	-3	(°C)
θ_l^u	0.1	
θ_i^u	0.15~0.35 *	

The initial ice content is determined by averaged daily maximum air temperature from January to April, illustrated in Fig. 7.

Table 5. Calibrated parameters.

Symbol		Value	Symbol		Value
T_1		−1	a_{nl}	*	1.5
T_2		−2		**	1.3
c_{rn}^{g}		0.7		***	0.4
c_2^{gT}		0.6	b_{nl}	*	1
c_{lg}^{gT}		0.6		**	0.6
ε_n^g	May	0.8		***	0.5
	June	0.6	T_0	*	0.4
	July	0.5		**	0.5
	August	0.4		***	3
k_1	May	0.1	Note		
	June	0.1	*	$T_a \geq 3^{\circ}C$	
	July	0.2	**	$3^{\circ}C > T_a \geq 0^{\circ}C$	
	August	0.2	***	$0^{\circ}C > T_a \geq -3^{\circ}C$	

Table 6. Evaluation merits.

Year	R^2	IVF	R_E
1990	0.80	0.02	0.24
1991	0.77	–0.12	0.25
1993	0.64	0.073	0.34
1994	0.79	0.03	0.29
1995	0.73	–0.19	0.26

HESSD
4, 3627–3686, 2007

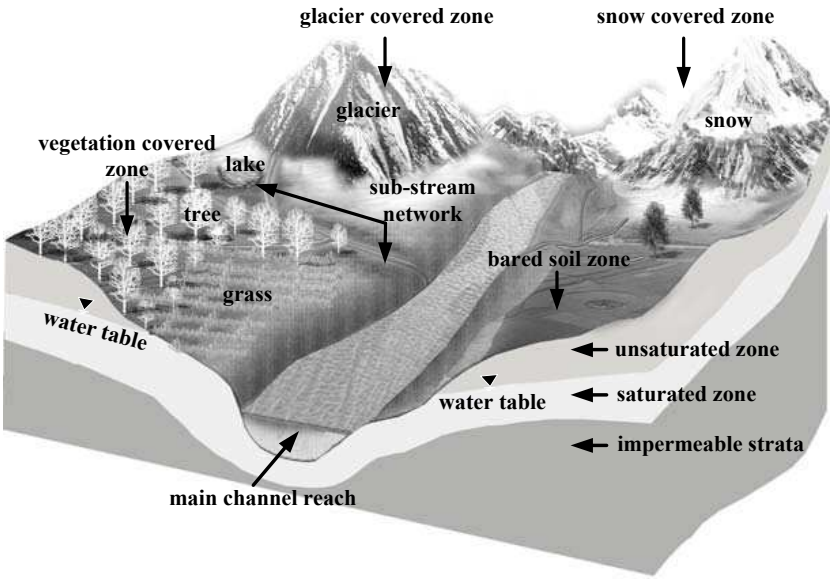

Fig. 1. Definition of REW after Tian et al. (2006a).

HESSD
4, 3627–3686, 2007

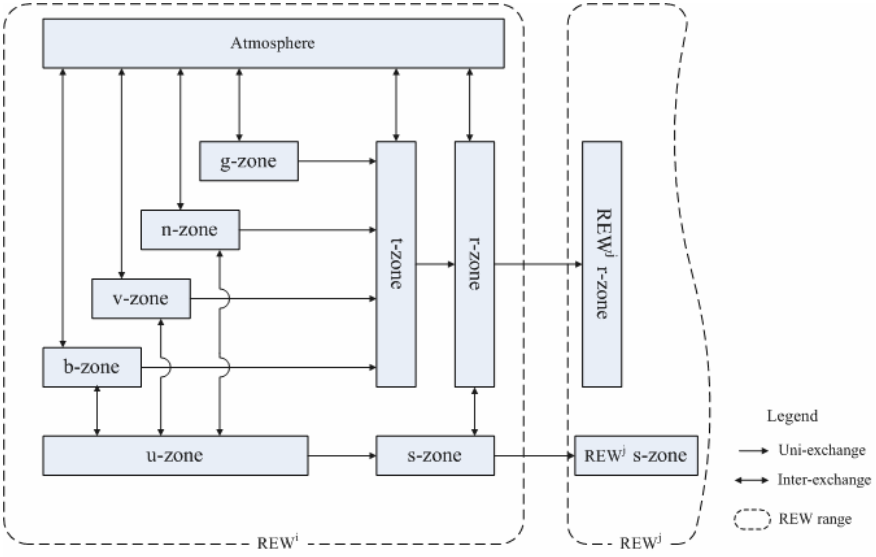

Fig. 2. Mass and energy exchange terms among sub-regions in cold regions.

HESSD
4, 3627–3686, 2007

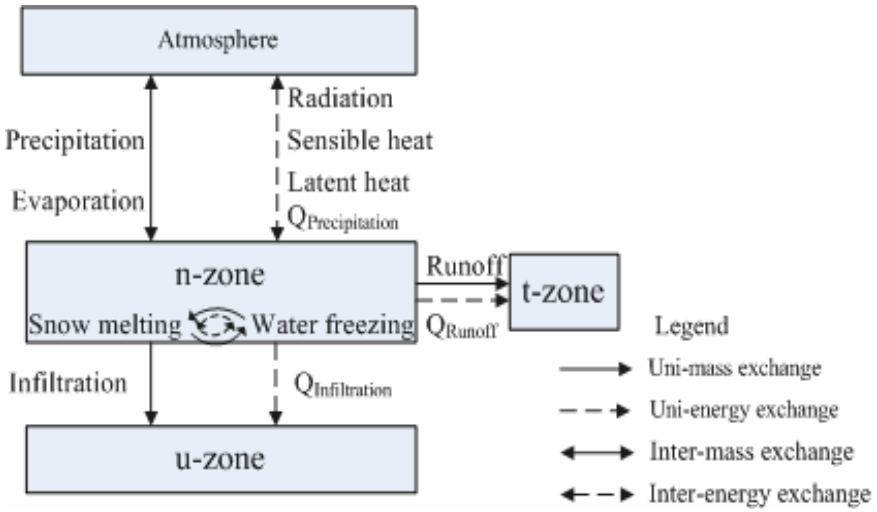

Fig. 3. Mass and energy exchange terms of snow covered zone.

HESSD
4, 3627–3686, 2007

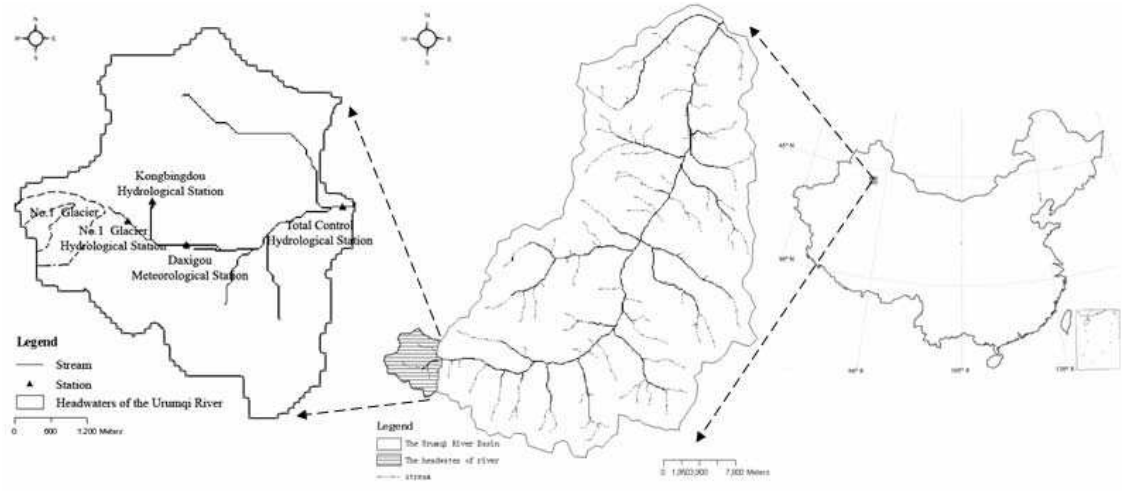

Fig. 4. The Urumqi River and its headwaters area.

HESSD
4, 3627–3686, 2007

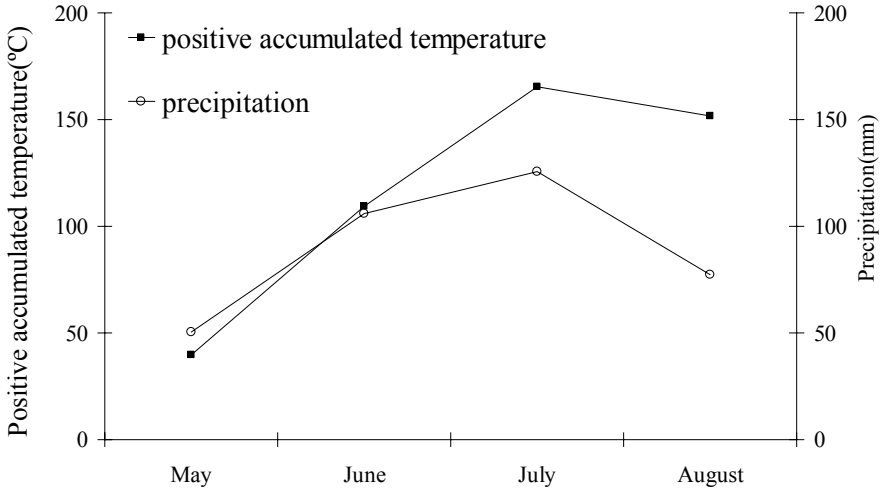

Fig. 5. Mean monthly precipitation and positive accumulated air temperature for headwaters of Urumqi River (according to the data measured at Daxigou meteorological station from 1990 to 2002).

HESSD
4, 3627–3686, 2007

EGU

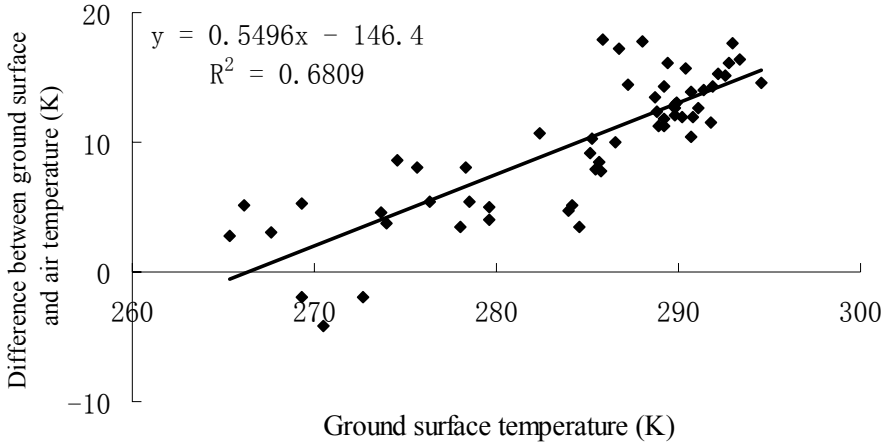

Fig. 6. Relationship between ground surface temperature and difference between daily mean air temperature and ground surface temperature.

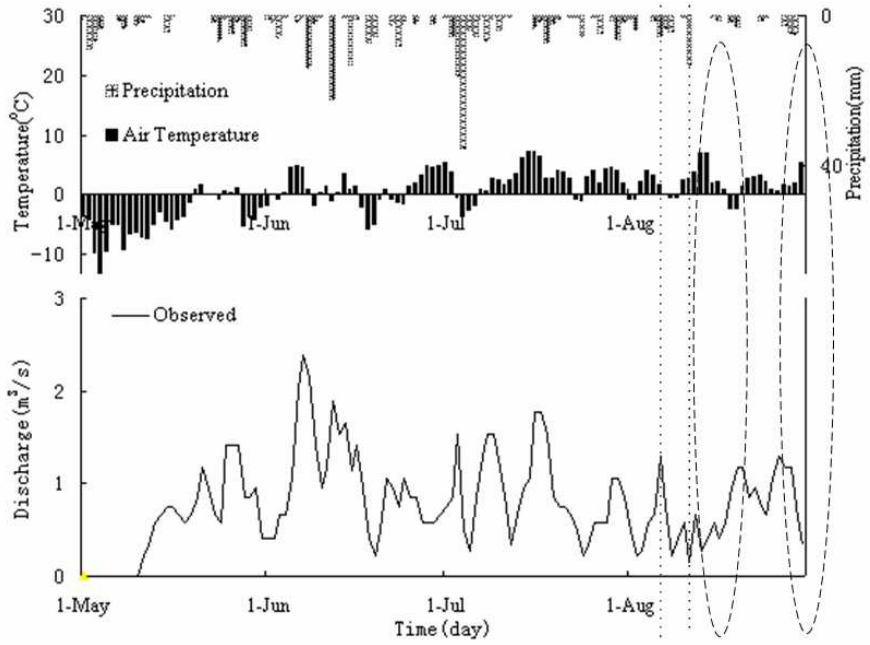

Fig. 7. Air temperature, precipitation and discharge in 1992.

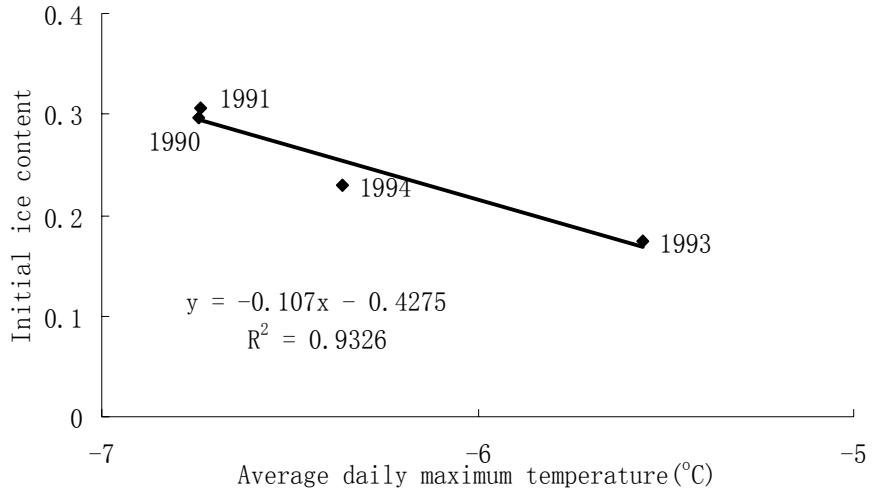

Fig. 8. Relationship between initial ice content and averaged daily maximum air temperature from January to April.

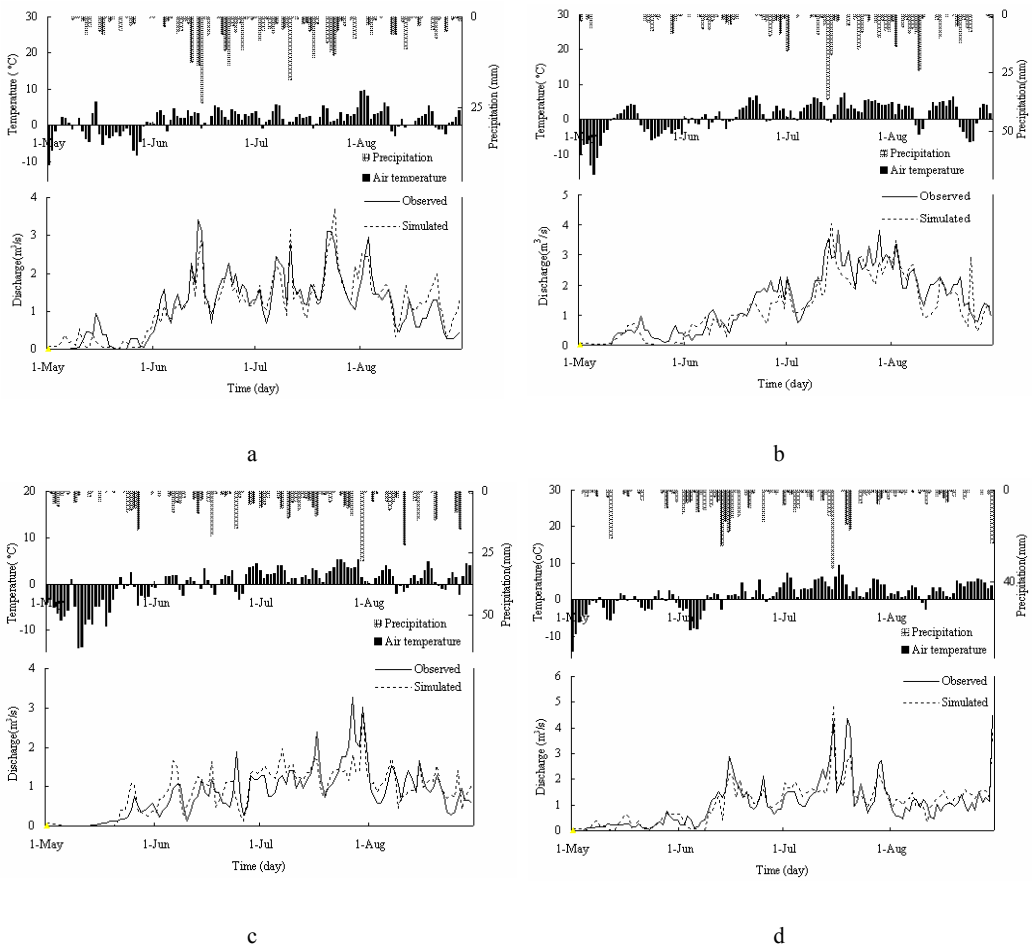

Fig. 9. Model calibration results (1) **(a)**, **(b)**, **(c)**, and **(d)** are hydrographs for 1990, 1991, 1993; and 1994.

HESSD
4, 3627–3686, 2007

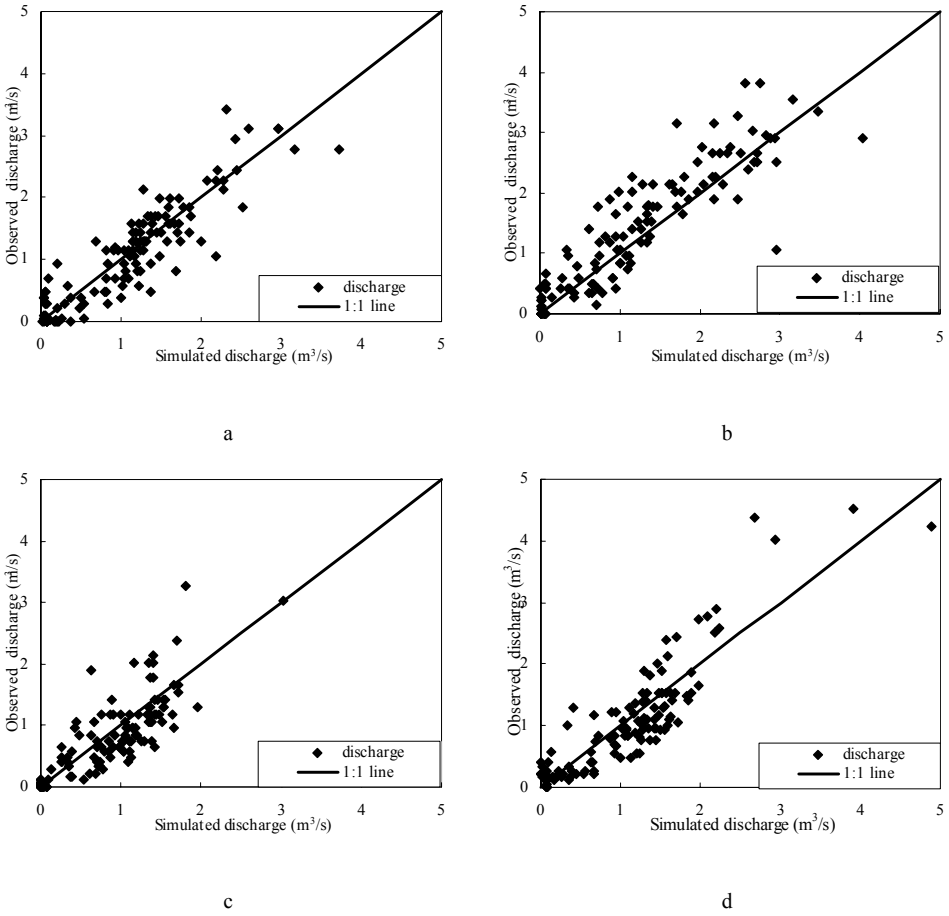

Fig. 10. Model calibration results (2) **(a)**, **(b)**, **(c)**, and **(d)** are correlation curve between observed and the simulated daily discharge for 1990, 1991, 1993, and 1994.

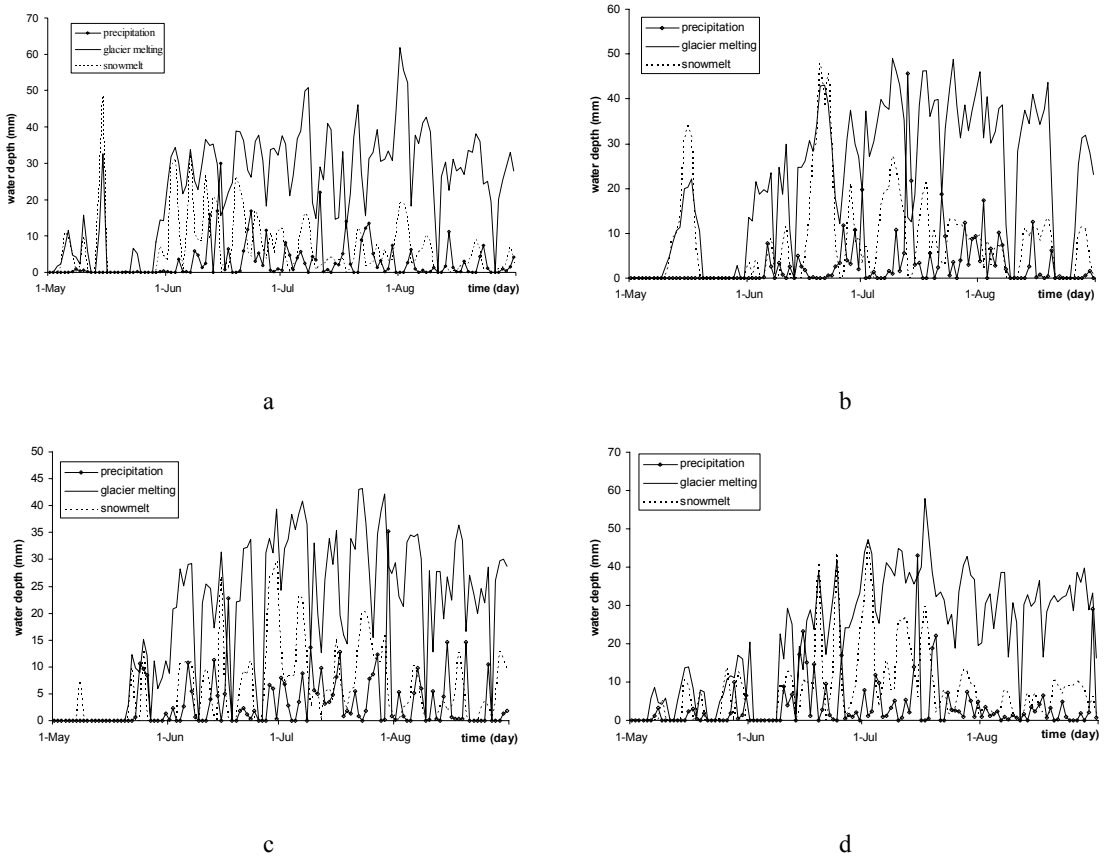

Fig. 11. Model calibration results (3) **(a)**, **(b)**, **(c)**, and **(d)** are daily water depth of glacier and snow melting and precipitation for 1990, 1991, 1993, and 1994.

HESSD
4, 3627–3686, 2007

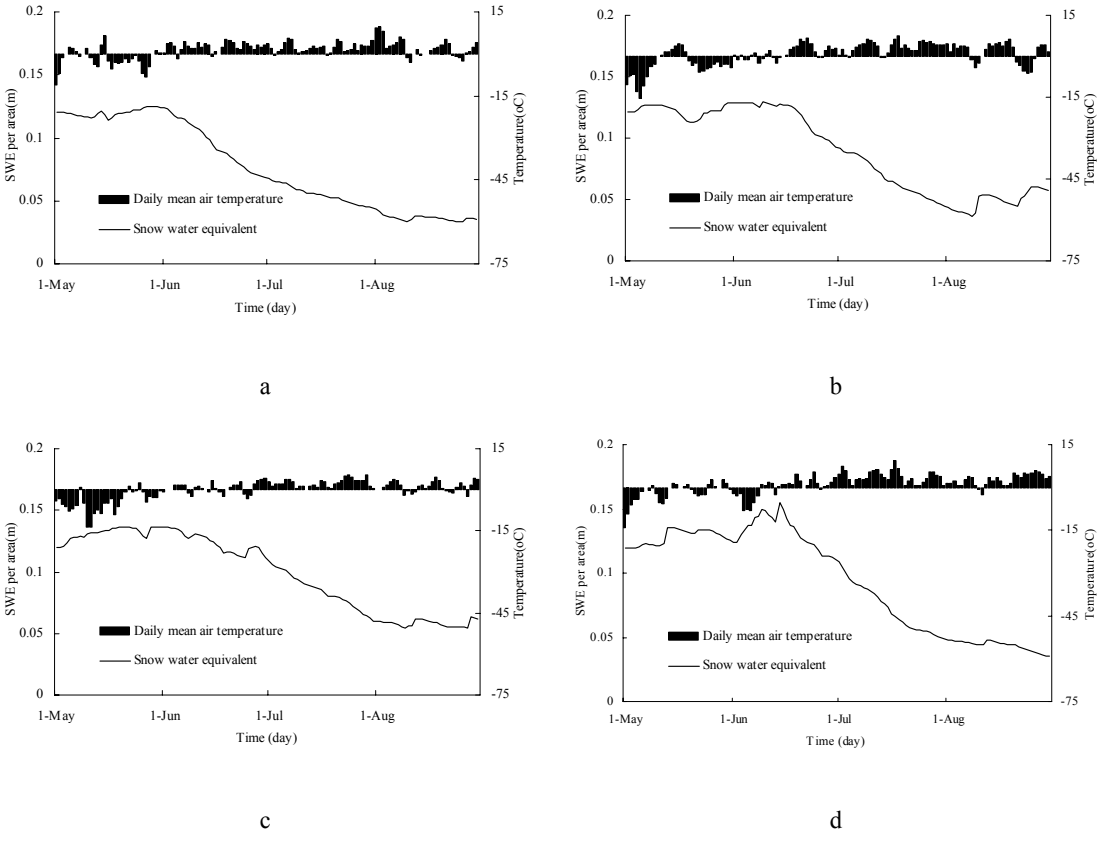

Fig. 12. Model calibration results (4) **(a)**, **(b)**, **(c)**, and **(d)** are daily SWE depletion/accumulation curve with daily mean air temperature for 1990, 1991, 1993, and 1994.

HESSD
4, 3627–3686, 2007

EGU

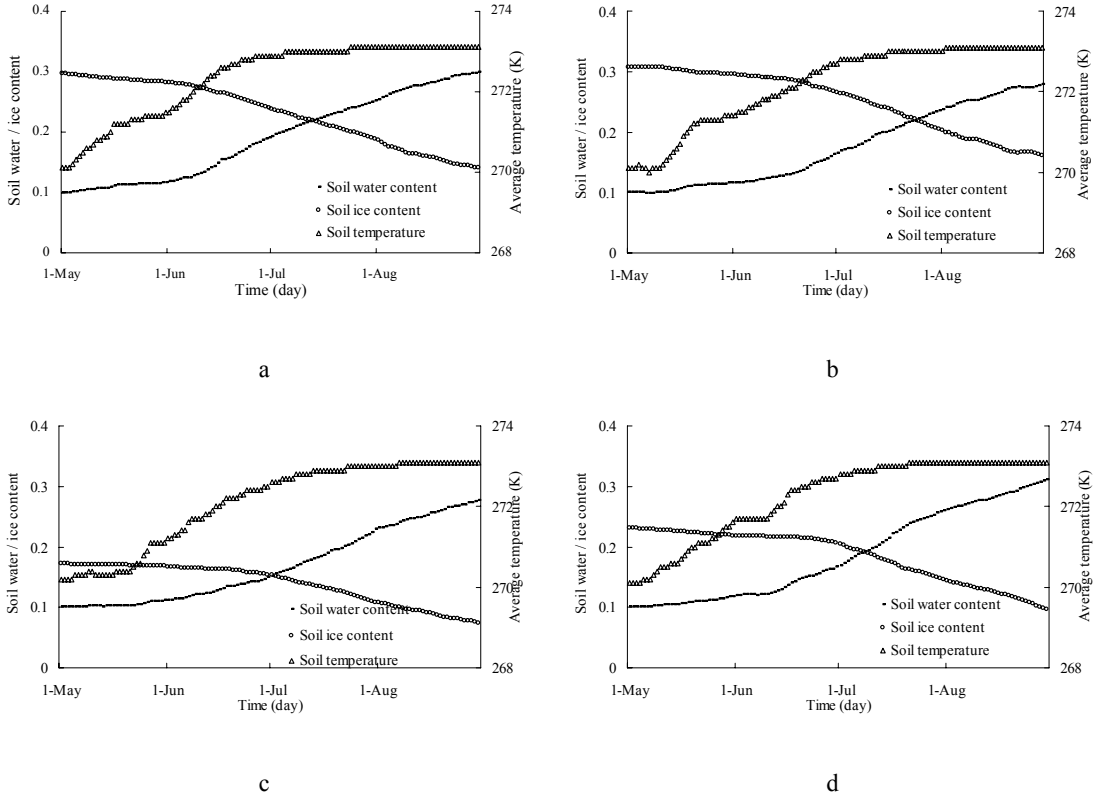

Fig. 13. Model calibration results (5) **(a)**, **(b)**, **(c)**, and **(d)** are soil water, ice and temperature dynamics for 1990, 1991, 1993, and 1994.

HESSD
4, 3627–3686, 2007

EGU

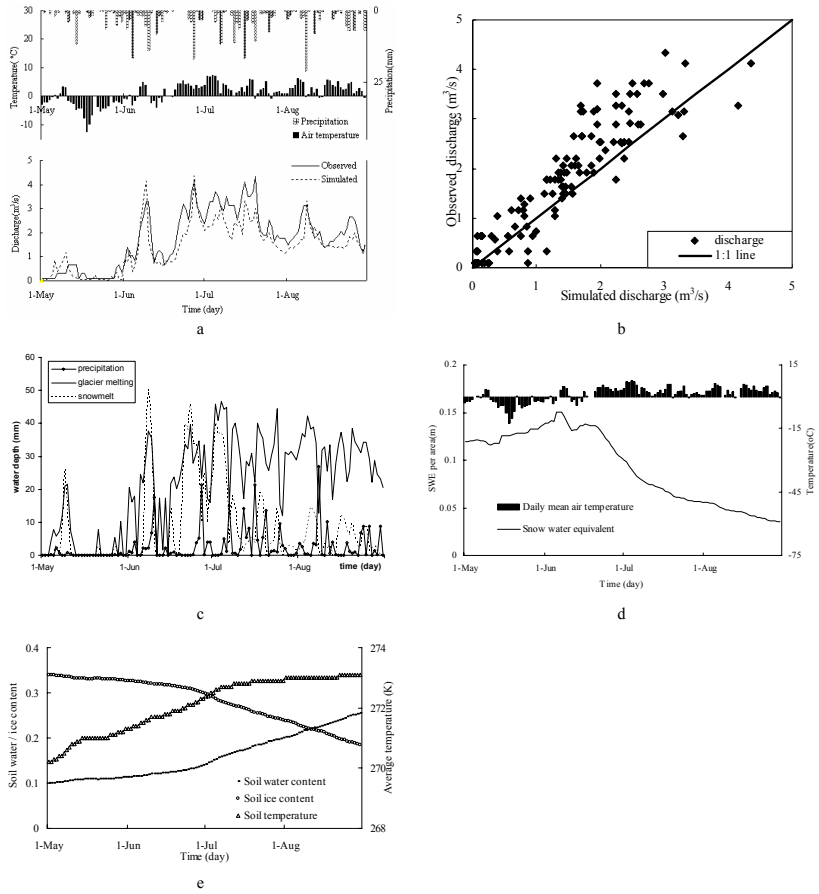

Fig. 14. Model validation results a ~ e are hydrographs, correlation between the observed and simulated discharge, daily water depth of glacier and snow melting and precipitation over the whole watershed, SWE change with daily mean air temperature and soil water, ice and temperature's change in 1995, respectively.

HESSD
4, 3627–3686, 2007

EGU